Design and Implementation of a Constant Envelope OFDM Waveform in a Software Defined Radio Platform

Amos Vershima Ajo Jr.

Thesis submitted to the faculty of the Virginia Polytechnic Institute and State University in partial fulfillment of the requirements for the degree of

Master of Science
in
Electrical Engineering

Carl B. Dietrich, Chair
A. A. (Louis) Beex, Chair
Allen B. MacKenzie

May 5, 2016
Blacksburg, Virginia

Keywords: OFDM, Constant Envelope OFDM, Peak-to-Average Power Ratio, Software Defined Radio, GNU Radio

Design and Implementation of a Constant Envelope OFDM Waveform in a Software Defined Radio Platform

Amos Vershima Ajo Jr.

ABSTRACT

This thesis examines the high peak-to-average-power ratio (PAPR) problem of OFDM and other spectrally-efficient multicarrier modulation schemes, specifically their stringent requirements for highly linear, power-inefficient amplification. The thesis then presents a most intriguing answer to the PAPR-problem in the form of a constant-envelope OFDM (CE-OFDM) waveform, a waveform which employs phase modulation to transform the high-PAPR OFDM signal into a constant envelope signal, like FSK or GMSK, which can be amplified with non-linear power amplifiers at near saturation levels of efficiency. A brief analytical description of CE-OFDM and its suboptimal receiver architecture is provided in order to define and analyze the key parameters of the waveform and their performance impacts.

The primary contribution of this thesis is a highly tunable software-defined radio (SDR) implementation of the waveform which enables rapid-prototyping and testing of CE-OFDM systems. The digital baseband processing of the waveform is executed on a general purpose processor (GPP) in the Ubuntu 14.04 Linux operating system, and programmed using the GNU Radio SDR software framework with a mixture of Python and C++ routines. A detailed description of the software implementation is provided, and baseband simulations of the SDR CE-OFDM receiver in additive white Gaussian noise (AWGN) validate the performance of the implemented signal processing.

A fully-functional CE-OFDM radio system is proposed in which GPPs executing the software defined transmitter and receiver routines are interfaced with Ettus Universal Software Radio Peripheral (USRP) transceiver front ends. A software ‘test bench’ is created to enable rapid configuration and testing of the CE-OFDM waveform over all permutations of its parameters, over both simulated and physical RF channels, to draw deeper insights into the characteristics of the waveform and the necessary design considerations and improvements for further development and deployment of CE-OFDM systems.

Design and Implementation of a Constant Envelope OFDM Waveform in a Software Defined Radio Platform

Amos Vershima Ajo Jr.

GENERAL AUDIENCE ABSTRACT

Orthogonal Frequency Division Multiplexing (OFDM) is a modulation scheme which has become virtually ubiquitous in the world of wireless communications; from the radio frequency (RF) signals transmitted to and from our Wi-Fi routers, to the RF signals transmitted to and from our mobile carrier's LTE cellular towers, the transmission and reception of OFDM signals has become nearly essential to our daily life. OFDM's virtues include its outstanding versatility and ability to deliver high-data rate communications over harsh mobile radio channels, but its primary downfall is the demand it makes for significant energy waste upon amplification. A novel modulation scheme called constant-envelope OFDM (CE-OFDM) is a unique solution power inefficiency problem of traditional OFDM, as it offers nearly optimal levels of power efficiency at the power amplifier (PA).

In this thesis, CE-OFDM is described qualitatively and analytically to, respectively, motivate an understanding of the waveform's advantages over traditional OFDM, and detail an implementation of a CE-OFDM transmitter and receiver in which the waveform's key performance-affecting parameters are easily tunable in software. Using software-defined radio (SDR), a paradigm of radio design in which a significant amount of dedicated circuitry in a radio is replaced with programmable hardware, a fully-functional, highly configurable, CE-OFDM radio system was implemented. This system forms a platform which can simultaneously simulate the performance of CE-OFDM in a purely-software environment, where its various nuances and performance over a variety of radio environments can be analyzed, and also interface with SDR RF hardware to implement real CE-OFDM radio links. The promise of this work is to enhance the knowledge of CE-OFDM waveform performance and behavior, shorten the lifecycle between the simulation and the implementation of CE-OFDM systems, and promote further research and development of CE-OFDM systems for a greener telecommunications industry.

ACKNOWLEDGEMENTS

I would like to give my deepest thanks to my advisor and committee chair, Dr. Dietrich for his mentorship, support, assistance and patience during the development of this thesis and throughout my graduate education at Virginia Tech. I would also like to express my gratitude to the members of my thesis committee, Dr. Beex and Dr. MacKenzie for offering their time, guidance, and critical insights.

I would like to especially thank Dr. Dietrich and Dr. Beex for inspiring me to pursue my graduate education at Virginia Tech, during my NSF Research Experience for Undergraduates (REU) Internship in the summer of 2013.

I would like express my deepest gratitude to Joe Molnar of the Naval Research Laboratory for providing me the opportunity to begin my research, and I would also like to thank Frank Fu and Andrew Robertson for their guidance and mentorship.

Finally but not the least, I would like to express my deepest appreciation for my Mom and Dad who have offered me unending love, support, and encouragement throughout my entire life, and vitally so during my graduate studies. I dedicate this thesis to them.

TABLE OF CONTENTS

GLOSSARY OF TERMS

3GPP	3rd Generation Partnership Project
ACI	Adjacent Channel Interference
ADC.	Analog to Digital Converter
AM	Amplitude Modulation
AM-AM	Amplitude-to-Amplitude Transfer Function
AWGN ……	Additive White Gaussian Noise
BER ……	Bit Error Rate
BPSK	Binary Phase-Shift Keying
C++ …….	C-Plus-Plus, programming language
CCDF	Complimentary Cumulative Distribution Function
CDM	Code Division Multiplexing
CNR	Carrier-to-Noise Ratio
CP.	Cyclic Prefix
CPU.	Central Processing Unit
CR.	Cyclic Redundancy Check
DAC	Digital to Analog Converter
DC	Direct Current
DDC	Digital Downconverter
DFT……..	Discrete Fourier Transform
DSL …….	Digital Subscriber Line
DSP	Digital Signal Processor
DUC	Digital Upconverter
EER	Envelope Elimination and Restoration
EM	Electromagnetic Wave
FDM	Frequency-Division Multiplexing
FEC…….	Forward Error Correction
FFT	Fast Fourier Transform
FIR	Finite-Impulse Response
FM	Frequency Modulation

FOBP	Fractional Out of Band Power
FPGA	Field-Programmable Gate Array
FSM	Finite State Machine
GHz…….	Gigahertz (1000 MHz)
GNU	“GNU’s Not UNIX” Open-Source Software System
GPP	General Purpose Processor
GRC	GNU Radio Companion
GUI	Graphical User Interface
i.i.d.	Independent and Identically Distributed
IBO	Input-Power Backoff
ICI	Inter-Carrier Interference
IDFT	Inverse Discrete Fourier Transform
IEEE.	Institute of Electrical and Electronics Engineers
IF	Intermediate Frequency
IFFT	Inverse Fast Fourier Transform
IIP3	Third-Order Intercept Point
IIR	Infinite-Impulse Response
IMD	Intermodulation Distortion
ISM	Industrial, Scientific and Medical
kHz	Kilohertz (1000 Hz)
LAN.	Local Area Network
LINC	Linear Amplification in Nonlinear Components
LTE	3GPP Long Term Evolution
MAC.	Media Access Control
MHz……	Megahertz (1000 kHz)
ML.	Maximum Likelihood
OBO	Output-Power Backoff
OFDM	Orthogonal Frequency-Division Multiplexing
OOP ……	Object Oriented Programming
PAPR……	Peak-to-Average Power Ratio
PC.	Personal Computer

PDF……	Probability Density Function
PN	Pseudorandom Noise
PPM ……..	Parts Per Million
PSD	Power Spectral Density
PSK	Phase-Shift Keying
QAM	Quadrature Amplitude Modulation
QPSK	Quadrature Phase-Shift Keying
RAM.	Random Access Memory
RF.	Radio Frequency
RMS…….	Root Mean Square
SC-FDMA.	Single Carrier Frequency Division Multiple Access
SDR	Software Defined Radio
SER…… .	Symbol Error Rate
SNR	Signal-to-Noise Ratio
SWIG.	Simplified Wrapper and Interface Generator
USB	Universal Serial Bus
USRP	Universal Software Radio Peripheral
USRP N210	Universal Software Radio Peripheral Network-Series Model 210
VCO	Voltage-Controlled Oscillator
Wi-Fi	802.11 Wireless Local Area Network
WiMAX	Worldwide interoperability for Microwave Access
WLAN	Wireless Local Area Network
XML	Extensible Markup Language

LIST OF FIGURES

1 INTRODUCTION

1.1 Motivation

Orthogonal Frequency Division Multiplexing (OFDM) is a multi-carrier modulation scheme which has become virtually indispensable in the world of wireless communications. OFDM has been the physical layer backbone and key enabler for the development of some our most important wireless protocols, from the IEEE 802.11 standards for Wi-Fi to both the 3GPP Long Term Evolution (LTE) and IEEE 802.16 Wi-MAX standards for 4G cellular communications. The mathematical properties of OFDM make it a proverbial "Swiss army knife" for tackling some of the most constraining challenges of wireless radio communications, particularly in enabling high data rate communications over harsh mobile channels.

The multi-carrier nature of OFDM provides the modulation an inherent resilience to the frequency-selective fading effects characteristic of broadband multipath radio channels, far surpassing the multipath performance of its single-carrier (SC) modulation rivals. OFDM effectively reduces the impact of a broadband multipath channel to that of several narrowband, single-path subchannels – each requiring minimal, single-tap, equalization to compensate for multipath fading across the full signal bandwidth. The orthogonality of OFDM subcarriers enables the modulation to utilize bandwidth with greater efficiency, higher throughput and capacity than the traditional Frequency Division Multiplexing (FDM) techniques. OFDM also leverages this subcarrier orthogonality to enable such ingenious technologies as adaptive subcarrier allocation and bit-loading, as well as the OFDM multiple access (OFDMA) scheme which has become a foundation of the 4G standards. Moreover, the complex computations which OFDM requires can be executed with great efficiency using the fast Fourier Transform (FFT) algorithm and digital signal processor (DSP) hardware.

However, for the nearly perfect harmony that it orchestrates in enabling spectrally-efficient broadband wireless communications, OFDM generates an almost perfect storm for the crucial task of power amplification. As OFDM subcarriers combine additively, the OFDM signal experiences sporadic spikes of instantaneous signal power which, over a single symbol period, will commonly be more than 15 decibels (dB) above the average signal power [7] – this is called the peak-to-average-power ratio (PAPR) of a signal, and spectrally efficient OFDM modulations experience exceedingly high PAPR.

High PAPR signals require highly linear power amplification, and this demand for highly linear amplification presents the OFDM system designer with the fundamental power amplifier (PA) design tradeoff of choosing linearity versus efficiency. A highly linear PA is very expensive and also very power inefficient – wasting much of the DC power supply of the amplifier as heat during an RF cycle. Furthermore, even the most linear amplifiers are still non-linear devices and to avoid non-linear operation – specifically, the non-linear effects of amplitude distortion, spurious intermodulation distortion, and spectral regrowth - OFDM signals must be attenuated or "backed-off" to position their high-PAPR dynamic signal range within a sufficiently linear regime of the PA, before being presented to the PA input. This backoff breeds further wastefulness of precious power resources in the system. Various signal processing techniques for PAPR reduction exist to decrease the amount of power backoff required by OFDM, however these methods are often either distorting or add undesirable overhead, and do not address the fundamental inefficiency of a highly linear PA.

Constant-Envelope OFDM (CE-OFDM) has been suggested as a novel solution for PAPR-reduction in OFDM [1][2][11-13]. Via phase-modulation, CE-OFDM embeds the information contained in a high-PAPR message signal onto the phase of a carrier rather than its amplitude, resulting in an RF signal with a constant-envelope - an optimal 0 dB PAPR. This fundamentally eliminates the need for linearity throughout the entire RF signal processing chain, and as a result provides an incredibly green solution to the PAPR problem of OFDM. CE-OFDM signals can be amplified in the most efficient regimes of the most efficient PAs – providing an unsurpassed efficiency of power utilization to OFDM systems. The constant-envelope of CE-OFDM also eliminates the linearity burden on other nonlinear devices in the RF transceiver chain, such as analog-to-digital and digital-to-analog converters (ADC and DAC). These reasons make CE-OFDM an incredibly intriguing solution to the PAPR problem of OFDM and its multi-carrier variants.

1.2 Contribution

Much research has been conducted to establish theory for the performance of the CE-OFDM waveform, but still little fruit has come in the way of consideration for standardization and even system implementation. A litany of performance-affecting parameters and design considerations and tradeoffs must be judiciously weighted to perform fair and legitimate comparisons between

CE-OFDM and traditional PAPR-reduction solutions. While some research purports that the decided PAPR-reduction advantages of CE-OFDM make it a near good-as-advertised solution to the OFDM PAPR problem, others draw more pessimistic inferences due to some of its disadvantages, such as its purely real baseband signal requirement. This inconclusiveness has seemingly hindered the pace of adaption of CE-OFDM in the heavily-standardized field of OFDM-based research as well as efforts to move beyond theory and simulation into the design and hardware implementation of CE-OFDM systems.

This motivates the main purposes of this work:

1. Provide a fully-functional, highly tunable software-defined radio (SDR) implementation of a CE-OFDM waveform to enable rapid-prototyping of CE-OFDM systems.
2. Establish an experimental procedure for rapidly testing CE-OFDM systems over all permutations of its parameters, in both simulated and physical RF channels.

1.3 Organization

This thesis opens with 2 chapters of background. Chapter 2 provides fundamental context about software-defined radio (SDR), providing the reader a sufficient understanding of the basics of SDR and the SDR tools used in this thesis. Chapter 3 provides further background about OFDM, considering its essential characteristics, the mathematics which explains these, and details regarding practical implementation of OFDM systems. Chapter 4 considers the OFDM PAPR problem from a PA-perspective to motivate an understanding of the penalty it places on power inefficiency in OFDM systems. Chapter 5 introduces the CE-OFDM waveform as a very promising PAPR-reduction solution for OFDM, providing a breakdown of its fundamental parameters, a discussion of a sub-optimal CE-OFDM receiver architecture, a discussion of spectral and error-rate performance, and consideration of its fundamental characteristics and design tradeoffs. Chapter 6 is a description of the SDR implementation of a CE-OFDM system that details the hardware and software components of the SDR platform as well as the fundamental building blocks of the waveform and their software implementations. Chapter 7 describes the experimental methodology used to test and analyze the performance characteristics of the CE-OFDM waveform. Chapter 8 provides conclusions and practical design considerations drawn from the test results, and outlines a framework for further development of CE-OFDM research upon the SDR platform implemented in this work.

2 SOFTWARE-DEFINED RADIO BACKGROUND

This chapter is the first background chapter of the thesis. This chapter serves the purpose of introducing the basic concepts behind SDR, describing its hardware and software components, and introducing the SDR platform upon which this thesis was built.

2.1 SDR Concept

SDR is perhaps one of the most revolutionary, enabling technologies in the history of radio communications. SDR represents a paradigm for radio architectures in which the ADC and DAC are as close as possible to the antenna and where as much dedicated circuitry as possible is replaced by programmable digital hardware. The Figure 2.1 presents a simplified model of the SDR concept:

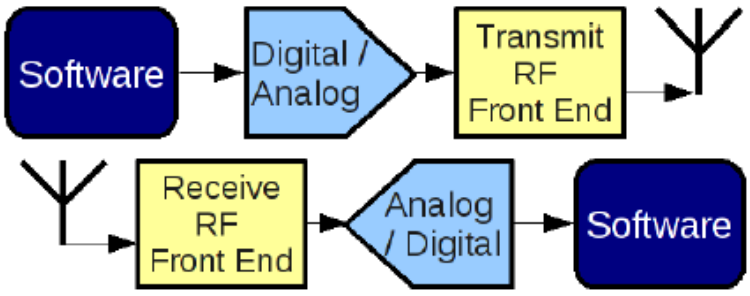

Figure 2.1: SDR Concept

The programmability of SDR hardware enables the design of radios whose modulation and demodulation signal processing can be completely defined in software, and can be paired with flexible RF front-ends to allow for multi-band transmission and reception. This programmability allows radio system designers to increase the decrease the cost and time of prototyping new radio system designs, as implementation of new systems consists of downloading new software rather than designing and fabricating new circuitry.

With this flexibility, SDR enables virtually endless possibilities in radio design. For instance, SDR designers can build radios which are programmed for interoperability between multiple standards and protocols. Such radios could be virtually future-proof, easily upgradable to the latest standards, and simultaneously retrogradable to older standards, all via simple software updates.

A more detailed model of the general SDR architecture is provided in Figure 2.2 [8]:

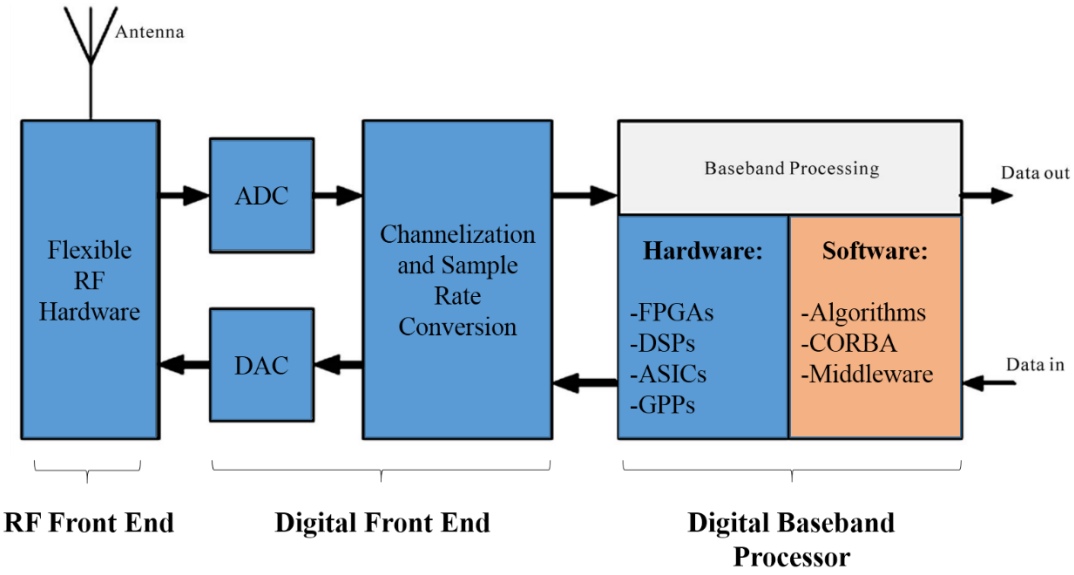

Figure 2.2: General SDR Architecture

The diagram in Figure 2.2 displays the fundamental components of the SDR architecture, namely the RF front-end, the digital front-end, and the digital baseband processor. In the following subsections, a brief discussion of some of the important concepts for both the hardware and software of SDR is provided.

2.2 SDR Hardware

The hardware components of an SDR exist in three categories: the RF Front-End, Digital Front-End, and Digital Baseband Processor. These hardware components are described in the subsections below.

2.2.1 SDR Radio Frequency Front-End

Starting from the left of the block diagram in Figure 2.2, the SDR architecture begins with its radio-frequency (RF) front-end. This is represented by the antenna and the 'Flexible RF Hardware' block in the diagram. The primary task of the RF front-end in an SDR transceiver is handling the over-the-air transmission and reception of an RF electromagnetic signal, and converting the signal to an appropriate frequency. In the receiver chain this means downconverting an RF signal to

baseband frequency, and in the transmitter chain this means upconverting a baseband analog signal to the appropriate RF frequency for transmission.

The RF front-end module for both receiver and transmitter will be composed of a chain of analog and digital circuits, including a number of filters, amplifiers, voltage-controlled oscillators (VCO), and phase-locked loops (PLL). The RF front-end is largely composed of dedicated circuitry, but many of these components are tunable and enable the reception and transmission of RF signals in multiple bands and at variable power levels [8].

2.2.2 SDR Digital Front-End

Connected to the SDR RF front-end is its digital front-end (DFE). Figure 2.2 shows the digital front-end module as being composed of ADC and DAC blocks and a channelization and sample rate conversion block. The purpose of the DFE is to interface between the SDR RF front-end and its digital baseband processor. In doing this, the DFE performs a couple major goals:

The first task of the DFE, in an SDR receiver, is to sample and digitize a downconverted baseband analog signal received by the RF front-end. This task is performed by an ADC, and the output will be a Nyquist-sampled, high sample-rate, digital signal representation of a broadband RF channel. The second task of the DFE is to select a desired channel from the broadband signal, *channelization,* and to reduce the high sample-rate of the signal to a minimum in order to avoid excessive computation in the digital baseband demodulator, *sample-rate conversion.*

In an SDR transmitter chain these processes occur in reverse: a minimally-sampled baseband signal is upsampled before being input to a DAC. The DAC produces the analog baseband signal to be upconverted and transmitted by the RF front-end.

2.2.3 SDR Baseband Digital Processor

The heart of an SDR can probably be considered to be its digital baseband processor. This is a programmable digital processor platform upon which real-time modulation and demodulation of digital baseband signals are performed. Signal processing routines such as digital filtering, encoding/decoding, interleaving/de-interleaving, and equalization are programmed in software instructions which are executed by the baseband processor.

One of a number of programmable digital processor architectures can be employed in SDR. These include digital signal processors (DSP), field-programmable gate arrays (FPGA), and general-

purpose processors (GPP). A choice of one of these digital processors typically requires a trade-off between performance, computational efficiency, and programmability. The choice of platform is an important decision, and based on the needs of the SDR designer. In this thesis, the implemented SDR employs a GPP in the form of a personal computer CPU as the hardware platform of the digital baseband processing unit.

2.3 SDR Software

The software component of an SDR describes the software instructions used to program the digital baseband processor. These instructions program the processor to perform the signal processing computations which modulate and demodulate an information-carrying, digital-baseband signal. A variety of SDR software development frameworks exist, but the software development environment chosen to implement the SDR of this thesis is called GNU Radio.

2.4 Proposed SDR Platform

Figure 2.3 displays a basic setup of SDR hardware and software which compose a fully functional radio system.

Figure 2.3: SDR System w/ USRP and GNU Radio

In Figure 2.3, an Ettus Universal Software Radio Peripheral (USRP), which contains RF and digital front end circuitry, is interfaced via gigabit Ethernet with a digital baseband processor in the form of a personal computer running GNU Radio applications.

Chapter 6 details the implementation of the baseband modulation and demodulation of a constant envelope OFDM waveform using the GNU Radio software. To begin an analysis of the waveform, Chapter 3 provides background of the OFDM multicarrier modulation scheme.

3 ORTHOGONAL FREQUENCY-DIVISION MULTIPLEXING BACKGROUND

OFDM, Orthogonal Frequency-Division Multiplexing, is a modulation technique which has revolutionized the wireless communications industry. OFDM is a multicarrier scheme, which divides a wideband signal into multiple narrower bands of spectrum such that the aggregate signal does not suffer the total impact of the fading in a wideband multipath channel. This lends OFDM its inherent ability to enable high-speed communication on harsh wideband multipath channels without the need for complex channel equalization. This virtue has made OFDM a favorite modulation technique for 802.11 Wi-Fi protocols, and the 4G cellular standards, which must support wideband data traffic over wireless channels.

This chapter presents the critical properties of OFDM. It begins with a cursory treatment of the impairments caused by multipath channels and their representations in both the time and frequency domain, and continues with an analytical description of OFDM and the properties which build its immunity to multipath fading effects. The digital implementation of OFDM along with its various benefits is then discussed before a consideration of its chief drawback- namely the PAPR problem.

3.1 Multipath Fading Phenomena

In a multipath channel, a transmitted signal will be reflected and scattered along multiple paths which arrive at the receiver at different times and with different amplitudes. Figure 3.1 pictorially represents the multipath scatterers of a signal in a wireless channel.

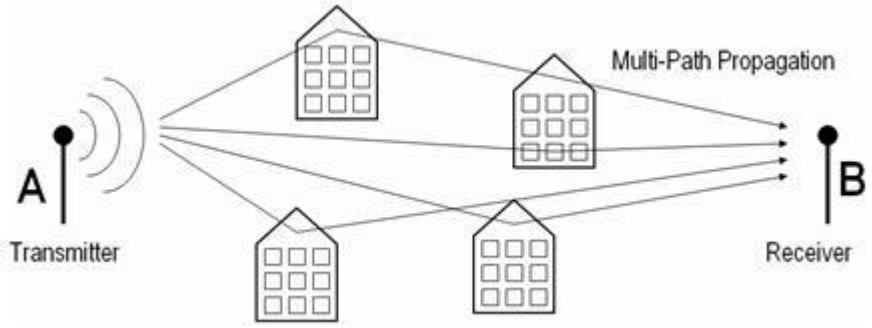

Figure 3.1: Multipath Signal Propagation

When the incident path, or the earliest-arriving signal, arrives at the receiver it is combined with energy from multiple delayed reflections of itself. For this reason, the channel is said to *spread* the

signal in time. This results in a harmful, fluctuating distortion on the amplitude of the incident signal - an effect called *multipath fading*.

While multipath fading can critically impair many communication systems, the properties of OFDM signals allow them to endure multipath fading with considerable grace. To understand how OFDM performs it is helpful to consider the frequency and time-domain properties of a multipath channel, and then the frequency and time-domain properties of an OFDM signal.

3.1.1 Time-Domain Representation of a Multipath Channel

The time-domain impulse response function of a multipath channel, $h(t)$, is displayed in Figure 3.2.

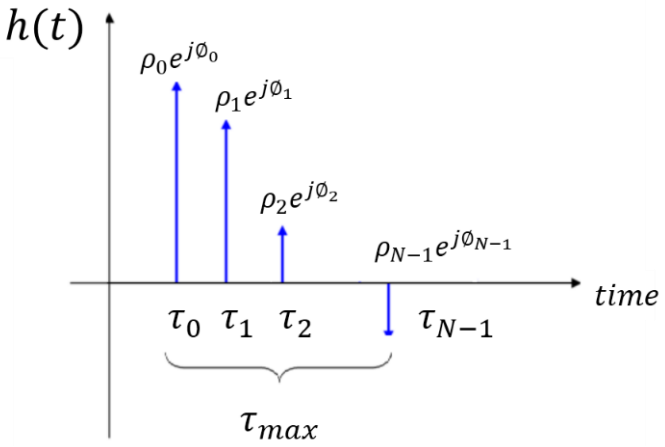

Figure 3.2: Multipath Channel Time-Domain Impulse Response

A channel which produces N scatter paths has a time-domain channel response that is the summation of N Dirac-impulses, each with a delay τ_i, and an amplitude $\rho_i e^{j\emptyset_i}$, which respectively correspond to the delay and gain of the signal on each path:

$$h(t) = \sum_{i=0}^{N-1} \rho_i e^{j\emptyset_i} \delta(t - \tau_i) \tag{3.1}$$

Figure 3.2 shows a metric of the channel, τ_{max}, called the *delay spread* of the channel. τ_{max} is equal to the difference between the time-of-arrival of the earliest and latest-arriving paths of the channel, and is one measure of the severity of multipath fading in the channel. τ_{max} describes the

duration over which signal's energy will continue echoing, or spreading, in the channel after it has been received on the incident path [17].

3.1.2 Frequency-Domain Representation of a Multipath Channel

In the frequency domain, the multipath channel will be represented by a frequency response as displayed in Figure 3.3.

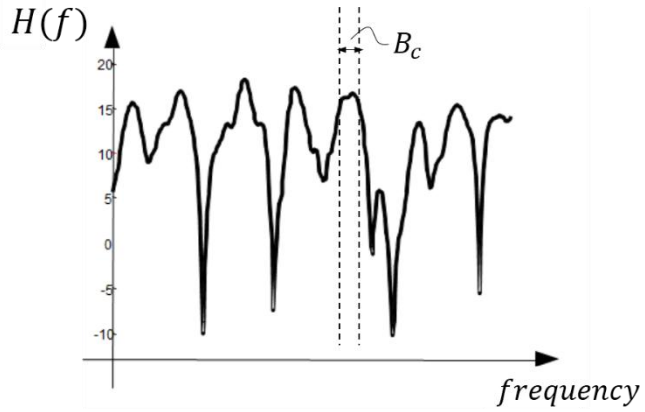

Figure 3.3: Multipath Channel Frequency-Domain Response

The frequency-response of a multipath channel $H(f)$, is the Fourier transform of the time-domain impulse response of the channel $h(t)$. An ideal, single-path channel consists of a single Dirac-impulse in the time domain, and thus a perfectly flat frequency response over all frequencies, in the frequency domain – this is not the case for multipath channels. As shown in Figure 3.3, multipath channels exhibit intermittent dips or fades at certain frequencies. Figure 3.3 also shows a metric of the channel called the *coherence bandwidth*, B_c. B_c is defined as the largest bandwidth over which the frequency response of the channel remains flat.

3.1.3 Impairments of Multipath on Single-Carrier Modulation

Single-carrier (SC) modulation schemes modulate digital symbols serially upon a single, high-frequency carrier. The spectrum of an SC-modulated symbol will be centered at the frequency of the carrier with a bandwidth W, roughly equal to the symbol rate R_s, of communications. High data rate communication is thus synonymous with broadband, or wide bandwidth, communication. Considering the frequency response of Figure 3.3, the wireless multipath channel is not very kind to broadband communications. The narrowband B_c in a multipath channel is the maximum

bandwidth that a signal can occupy in order to observe a flat-frequency response. This means that the wideband symbols of high-speed SC modulation ($W \gg B_c$) will be deeply, possibly irreparably, distorted in a phenomena called *frequency-selective fading*.

The effect of frequency-selective fading on wideband SC modulated symbols can also be considered in the time-domain. SC symbols are transmitted serially with symbol time $T_s = 1/R_s$. Broadband SC communications transmit very short symbols, and if T_s is smaller than the delay spread of the channel τ_{max}, then the full duration of a received symbol, beginning on its arrival at the receiver along the earliest path, will be incident with energy from delayed reflections of previously transmitted symbols. This is observed in the Figure 3.4.

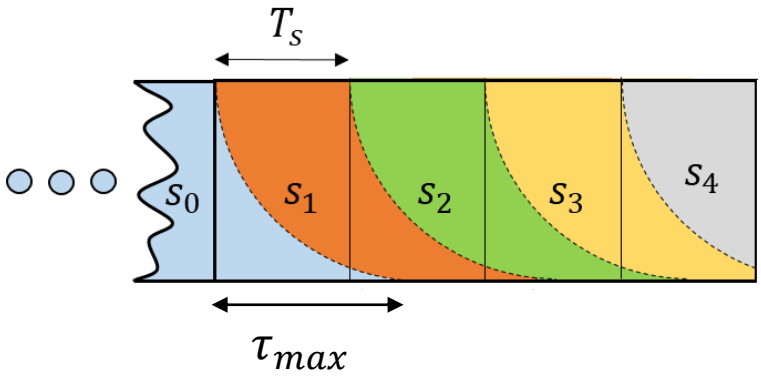

Figure 3.4: Inter-Symbol Interference on Short Symbols

This effect is called *inter-symbol interference* (ISI), in which energy from previous symbols spreads into the interval of a new symbol. The ratio $\frac{\tau_{max}}{T_s}$, the delay spread of the channel in units of symbol-times, is a good measure for the impact of ISI distortion on a digital signal. Because of the brevity of their symbols, the ISI length of a broadband SC modulation will often be greater than one full symbol-time.

The effects of ISI in the time-domain and selective fading in the frequency-domain are equivalent ways to describe the impairments of a multipath channel. Mitigation of these impairments is aimed for in a process called *channel equalization* and is a fundamental challenge of wireless communication systems. In very harsh multipath channels, ISI and frequency-selective fading can make the task of equalization extremely complex and even impossible. The properties of OFDM, however, enable broadband, high-speed communications over even such channels, with minimal equalization. These properties are considered in the following section.

3.2 OFDM in Multipath Channels

The key factor in the multipath resilience of OFDM is the use of multicarrier (MC) modulation. Figures 3.5 and 3.6 represent the difference between MC and SC modulation schemes in the frequency domain.

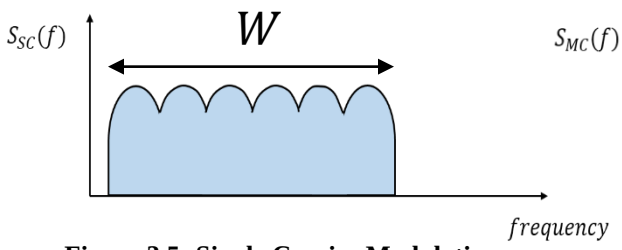

Figure 3.5: Single Carrier Modulation

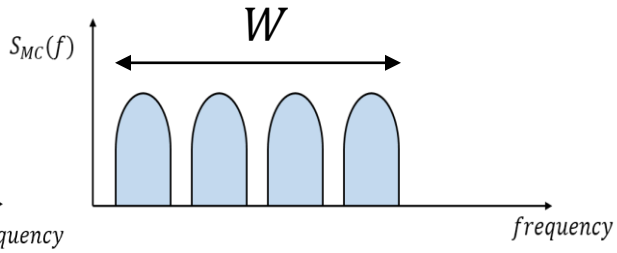

Figure 3.6: Multi-Carrier Modulation

As illustrated in Figure 3.6, MC modulation divides a wideband channel with bandwidth W into multiple, adjacent subchannels, each given a narrow bandwidth of W/N. While SC modulation transmits individual symbols serially on a single-carrier in the center of a wideband channel, MC modulation transmits N symbols in parallel, over N subcarriers centered in narrowband subchannels. In a system such as shown in Figure 3.6, a critical challenge becomes ensuring that adjacent subchannels of the MC signal do not overlap, to avoid inter-carrier interference (ICI). OFDM improves upon this technique by using subcarrier signals that are orthogonal, and leverages the fact that orthogonal signals may overlap in frequency without incurring ICI upon each other. As displayed in Figure 3.7, the allowance of subchannel overlapping yields OFDM greater spectral efficiency than typical FDM modulation.

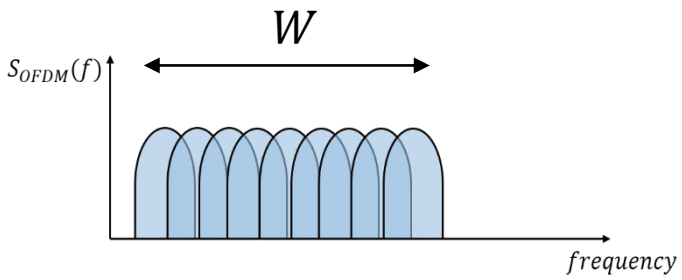

Figure 3.7: OFDM Modulation

3.2.1 Frequency-Selective Fading Immunity of OFDM

OFDM subcarriers are packed tightly in frequency with a separation, $\Delta f = W/N$, where N is equal to the number of OFDM subcarriers. OFDM systems can be designed with N large enough such that Δf, which is also the effective bandwidth of subchannels, becomes less than B_c of a multipath channel. In this way, each of the narrowband OFDM subchannels will observe a relatively flat channel-response. The figure 3.8 shows how OFDM divides a wideband multipath channel with bandwidth W into $N, \Delta f$ wide subchannels, the fading on each of which can be equalized very simply with single-tap equalizers.

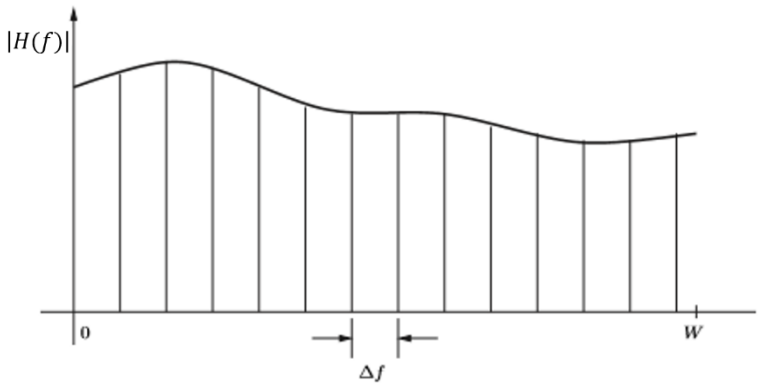

Figure 3.8: Subchannelization of Wideband Multipath Channel

3.2.2 Inter-Symbol-Interference Immunity of OFDM

The narrowband subcarriers of OFDM require long symbol durations. To satisfy orthogonality it is necessary that the symbol duration of each OFDM subcarrier be related to its frequency separation by, $T_s = 1/\Delta f$. Because $1/\Delta f = N/W$, this means that the duration of one aggregate

OFDM symbol is N times greater than that of a SC modulation. However, because OFDM transmits N symbols in parallel, the effective symbol rate of the two modulations remains the same. Figure 3.9 displays the way that the long OFDM symbol times dramatically decrease the ISI length of the channel.

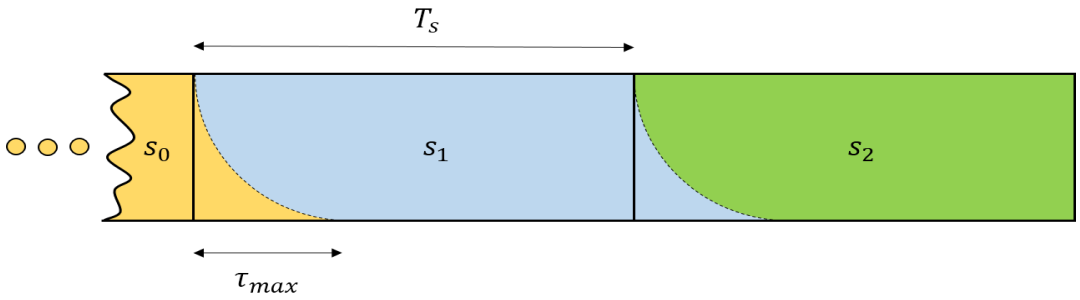

Figure 3.9: ISI Compensation with Long Symbols

When the ISI length is less than one-tenth of a symbol time, the effect of ISI is nearly nullified. OFDM can even better this by appending each symbol with an ISI-length buffer signal called a cyclic prefix which absorbs the ISI from the channel. Figure 3.10 displays how the addition of a cyclic-prefix (CP) can completely negate the effect of ISI at the cost of slightly reduced throughput.

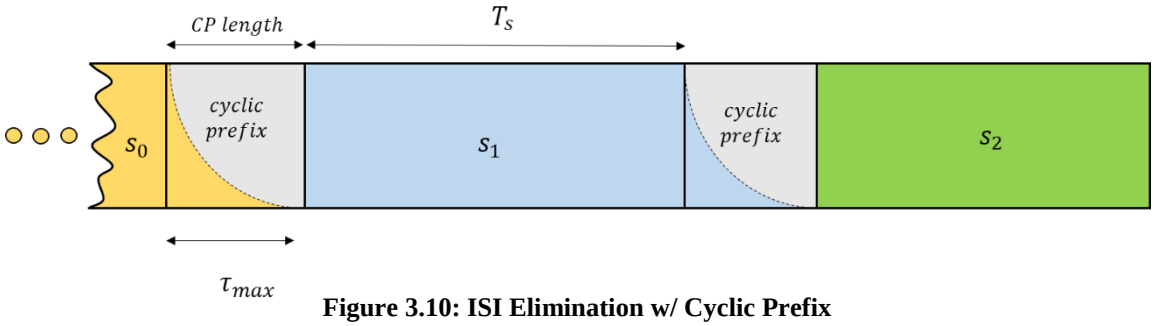

Figure 3.10: ISI Elimination w/ Cyclic Prefix

3.3 Analytical Description of OFDM

An analytical expression for a baseband OFDM signal is given as:

$$s(t) = \sum_{i} \sum_{k=0}^{N-1} I_{i,k} e^{j2\pi k \Delta f (t - iT_s)}$$

$$= \sum_{i} \sum_{k=0}^{N-1} I_{i,k} e^{j\frac{2\pi k}{T_s}(t - iT_s)} \qquad (3.2)$$

This expression shows that in the ith symbol interval, the OFDM signal will be composed of a summation of N subcarriers $\{e^{j\frac{2\pi kt}{T_S}}\}_{k=0}^{N-1}$, each modulated by a different symbol $I_{i,k}$. The subcarrier expression in (3.2) shows that the frequency of each complex sinusoid in the summation is a multiple k of the frequency separation Δf. This property ensures that all subcarriers in the set are mutually orthogonal signals:

$$\frac{1}{T_s}\int_0^{T_s}\left(e^{j2\pi f_{k_1}t}\right)\cdot\left(e^{-j2\pi f_{k_2}t}\right)dt = \frac{1}{T_s}\int_0^{T_s} e^{j2\pi(f_{k_1}-f_{k_2})t}dt \qquad (3.3)$$

$$= \begin{cases} 0, & k_1 \neq k_2, \\ 1, & k_1 = k_2, \end{cases}$$

$$\text{where, } f_{k_i} = k_i\Delta f = k_i/T_s$$

3.3.1 Digital Implementation of OFDM

One of the greatest luxuries of OFDM is its ability to be processed completely in the digital domain with digital hardware, using the FFT algorithm. The discrete-time expression for a Nyquist-sampled OFDM symbol, sampled at N equally-spaced time instances is given by:

$$s[n] \equiv s(t)|_{t=\frac{nT_s}{N}} = \sum_{k=0}^{N-1} I_{0,k}e^{\frac{j2\pi kn}{N}}, \quad n = 0, 1, \ldots N-1 \qquad (3.4)$$

The set $\{I_{0,k}\}_{k=0}^{N-1}$ is the set of symbols which modulates the N subcarriers of the OFDM symbol group. Equation (3.4) shows that the discrete-time OFDM baseband signal $s[n]$ is equivalent to the inverse Discrete Fourier Transform (IDFT) of the symbol vector $\{I_{0,k}\}_{k=0}^{N-1}$, the elements of which are the N parallel symbols which modulate the N OFDM subcarriers. Thus the synthesis and modulation the N orthogonal OFDM subcarriers is conveniently performed by an IDFT. The IDFT is equivalently processed with greater computational efficiency by the inverse Fast-Fourier Transform (IFFT) algorithm. With the addition of the cyclic prefixing, Figure 3.11, displays a block diagram of the baseband OFDM transmitter.

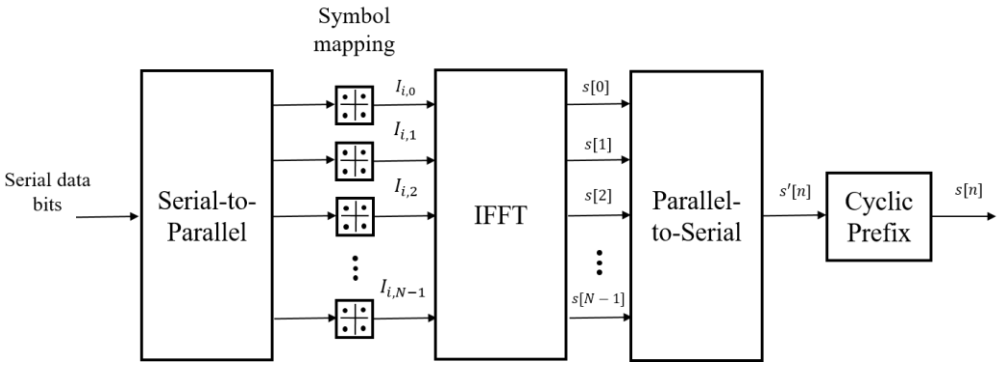

Figure 3.11: OFDM Transmitter Block Diagram

The OFDM receiver can recover the transmitted symbols $\{I_{0,k}\}_{k=0}^{k=N-1}$ by performing a forward-FFT on $s[n]$, a process which inverts the subcarrier modulation of the OFDM symbols:

$$I_{0,k} = \sum_{n=0}^{N-1} s[n] e^{-j2\pi kn/N} \tag{3.5}$$

With the added step of cyclic prefix removal, Figure 3.12 displays a block diagram of the baseband OFDM receiver:

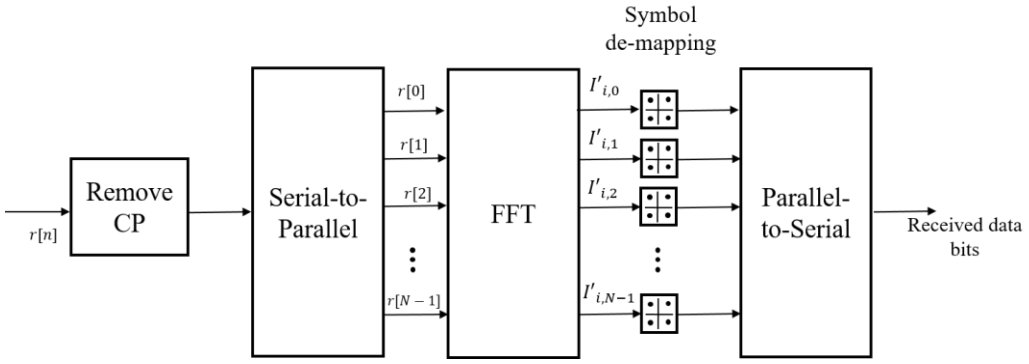

Figure 3.12: OFDM Receiver Block Diagram

The cyclic prefixing step in the OFDM transmitter is performed in the digital domain, by appending the last L samples of a symbol to the beginning of the symbol. If L samples last longer in time than the channel delay spread, $(L\frac{T_s}{N} > \tau_{max})$, then the cyclic prefix has the effect of absorbing the ISI energy away from the symbol. The choice of the last L samples as the cyclic

prefix is made because doing so has the effect of making the received symbol *circularly-convolutional* with the channel, which is necessary so that traditional methods of channel estimation and discrete-domain equalization may be performed on the OFDM symbols.

3.4 Benefits of OFDM

The description of the OFDM modulation technique in the preceding sections motivates an understanding of some of its truly graceful properties. Below, a brief point-by-point summary is provided of the various benefits which have made OFDM a mainstay in the wireless communications industry for the past decade:

- With minimal equalization, OFDM enables faithful broadband communications even over the erratic frequency selectivity of wideband RF multipath channels.
- Subcarrier orthogonality of OFDM allows for the dense packing of subcarrier symbols into an allotted bandwidth to improve overall spectral efficiency with respect to traditional FDM modulation.
- Subcarrier orthogonality of OFDM enables a host of practical PHY and MAC layer technologies
    - Adaptive bit-loading, which allows OFDM systems to weight data throughput toward subcarrier channels with better flat-channel characteristics
    - Power allocation, which allows OFDM systems to weight transmission power towards subcarrier channels with poorer flat-channel fading
    - Flexible designation of subcarrier duties: control subcarriers, guard subcarriers, synchronizing subcarriers, channel sensing subcarriers, etc.
- OFDM modulators and demodulators can be implemented very simply with the FFT algorithm, which is readily performable with great efficiency on modern DSP chips.

These reasons have made OFDM a seminal enabler of the multimedia explosion of the early 21st century. From the 802.11 Wi-Fi protocols, to the 4G cellular standards, OFDM has played an indispensable role in enabling wireless networks to support high-speed, multi-media rich services. OFDM, and its multi-carrier variants, will continue to figure prominently in the foreseeable future of wireless communications due to the grace with which it handles some of the more troubling problems of broadband wireless systems.

As is true of any technology, OFDM is not without critical faults and design challenges. The benefits of OFDM must be reconciled with its inherently high peak-to-average power ratio (PAPR) – a dilemma often termed the PAPR problem. The purpose of the following chapter of this thesis is to motivate an understanding of OFDM's PAPR problem as well as its critical implications for the power efficiency of OFDM and its multicarrier variants, and its broader implications concerning the sustainability of an increasingly OFDM and multicarrier enabled generation of multimedia wireless communications.

4 THE PROBLEM OF PEAK-TO-AVERAGE POWER RATIO IN OFDM

For the harmony OFDM orchestrates in enabling broadband multipath communication, OFDM conducts a seemingly perfect storm for the job of power amplification. The key culprit in this matter is the high peak-to-power-ratio (PAPR). The PAPR of a signal is defined as the ratio of a peak instantaneous power to the average power of a signal:

$$PAPR\{x(t)\} = \frac{peak\ signal\ power}{average\ signal\ power} = \frac{\max\{x^2(t)\}}{E\{x^2(t)\}}$$

In Section 4.1 a qualitative and quantitative discussion of the OFDM PAPR problem is provided, in Section 4.2 a discussion of power amplification of OFDM is provided to detail the impact of high PAPR amplification on power efficiency, and Section 4.3 closes with a discussion of the implications of the power inefficiency of OFDM.

4.1 PAPR Statistics of OFDM

In modulated RF signals, PAPR describes how greatly the signal *envelope*, the amplitude of its baseband signal, fluctuates. Because OFDM is composed of a summation of several linearly modulated subcarriers, whose amplitudes combine constructively and destructively, OFDM signals yield a highly erratic envelope and a very high PAPR. This means that while on average the OFDM signal power is relatively low, the signal will exhibit intermittent, high-powered spikes. This is displayed in Figure 4.1.

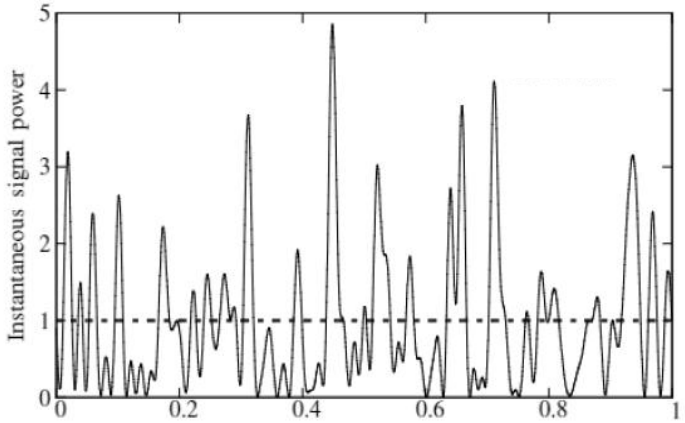

Figure 4.1: Instantaneous OFDM Signal Power over Symbol Period

The PAPR of an OFDM signal depends mainly upon two factors: N, the number of OFDM subcarriers, and M, the modulation order on the subcarriers. If N is chosen to be very large, a

design choice which increases spectral efficiency, the OFDM signal envelope will exhibit large spikes whenever a majority of the subcarrier symbol amplitudes combine constructively.

If subcarriers are modulated on a constant envelope, such as via phase-shift keying (PSK), the OFDM signal reaches its absolute peaks in the event that all N symbols align in phase. If the subcarriers are modulated with a non-constant envelope, such as with the highly spectrally-efficient M-ary QAM modulation, the OFDM peaks are magnified yet further and reach absolute crests when all symbols align in-phase, at their highest order amplitudes. In summary, *the more spectrally efficient the modulation is, the higher the PAPR will be*. Table 4-1 provides values of PAPR for various OFDM modulation parameters [7]:

Table 4-1: PAPR comparison for different OFDM modulation parameters

	$QPSK$	$16QAM$	$64QAM$	$256QAM$
$N = 64$	18 dB	20.4 dB	21.4 dB	22 dB
$N = 128$	21 dB	23.6 dB	24.6 dB	25.2 dB
$N = 256$	24 dB	26.5 dB	27.6 dB	28.1 dB
$N = 512$	27 dB	29.6 dB	30.7 dB	31.2 dB
$N = 1024$	30 dB	32.6 dB	33.7 dB	34.2 dB

The PAPR values in Table 4-1 tell a worst-case scenario for these OFDM signals, as they give a ratio of the *absolute* peak power to the average power. The event of absolute peaks occurring will be very rare if transmitted symbols can be modeled as independent and identically distributed (i.i.d) random variables. Hence more relaxed measures of signal dynamic range are often used such as the complementary cumulative distribution function (CCDF) of PAPR. Without loss of generality, however, PAPR is used to motivate the forthcoming discussion, and the next section of the chapter describes the impact of the OFDM's high PAPR on the efficiency of its power amplification.

4.2 Power Amplification of High-PAPR OFDM

Power amplification is a necessary stage in all wireless communications, as signals must be given enough power to carry their message over a required distance with a required fidelity. The greatest significance of the PAPR of a modulated signal is that the PAPR significantly affects the ability of the signal to be processed by non-linear components of the radio circuitry. In this

section the power amplifier (PA) is considered as one such non-linear element of critical importance, and the impact of high PAPR signal input on the power efficiency performance of a PA is considered. To begin a brief overview of the basic concepts of power amplification is in order.

4.2.1 Power Amplifier Basics

A PA can be generally characterized by the following parameters [15][20],

- Peak Output Power, $P_{out_{max}}$
- DC Power Supply, P_{DC}
- Drain Efficiency, η
- Linearity
- Gain

An ideal PA amplifies the input signal linearly by multiplying its amplitude with a fixed gain, but such a PA does not exist. A real PA is a nonlinear device with only limited regions of approximate linearity. The graph in Figure 4.2 shows the nonlinear amplitude-to-amplitude curve (AM-AM) of a PA. This curve displays the input signal power against the output signal power and describes many of the most important PA properties.

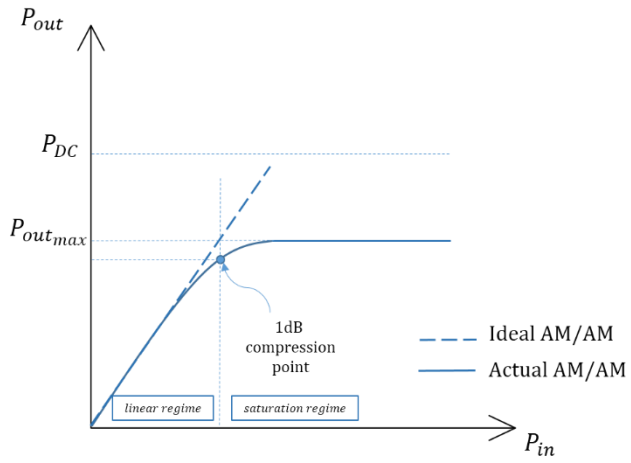

Figure 4.2: PA AM/AM Transfer Function

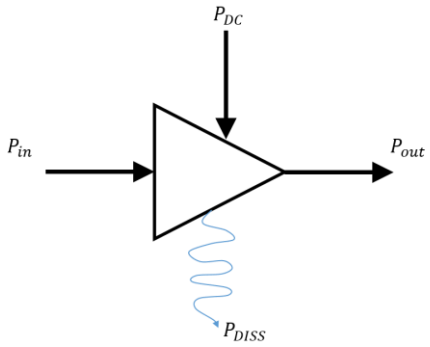

Figure 4.3: PA Simple Diagram

This provides a few critical figures of merit to discuss:

4.2.1.1 PA Operation Regions

The AM-AM curve in Figure 4.2 shows that a PA has a linear operation region in which the power of the output signal is approximately equal to the power of the input signal multiplied by the amplifier *gain*. The input signal can only be linearly amplified when its power is within a range called the *linear dynamic range*. The upper limit of this range is often characterized by the *1-dB compression point*, a point where the gain applied to the input power becomes 1 dB less than the nominal linear gain of the amplifier.

As the input signal power exceeds the linear dynamic range, the amplifier eventually reaches its *saturation region*, where its *peak output power* is reached, and no further amplification can be achieved.

4.2.1.2 PA Efficiency

Figure 4.3 provides a picture of the flow of power into and out of the PA. To amplify its input signal, a PA requires a *direct-current* (DC) *power supply* to provide energy to its active components (i.e. transistors). The *efficiency* of a PA, for which there are several metrics, describes how much of the DC power supply is used to produce the power of the output signal, and how much of the DC power is *dissipated* or lost as heat.

One common efficiency measure is called the *drain efficiency*, η_{drain}:

$$\eta_{drain} = \frac{P_{out}}{P_{DC}} \% \tag{4.2}$$

This ratio and the AM-AM curve helps to express that the efficiency of an amplifier is affected, predominantly, by two factors: the *region of operation* of the amplifier, and the linearity of *amplifier architecture:*

- *Region of operation*: From Equation (4.2) we see that η_{drain} of a PA is maximized when the output power is maximized $P_{out} = P_{out_{max}}$, that is, when the amplifier is operated within its saturation region. For this reason, η_{drain} is compromised when the PA operates within the linear region. Figure 4.4 displays this graphically. Here, two operating points a plotted along the AM-AM curve in the linear and saturation regions, respectively before and after the 1-dB compression point of the PA.

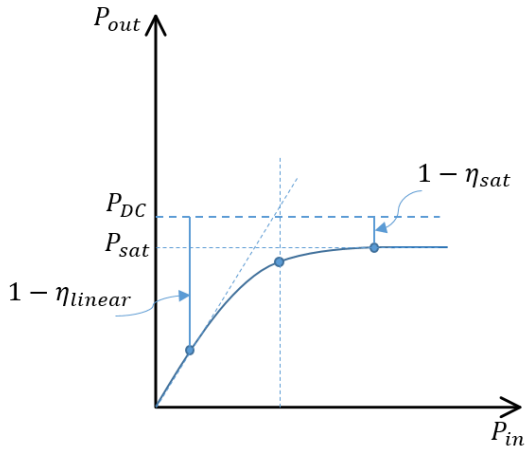

Figure 4.4: Effect of Operation Region on Drain Efficiency

The larger difference between P_{DC} and the linear operating point corresponds to a low drain efficiency, η_{linear}, and the small power difference between P_{DC} and the saturation power, $P_{sat} \equiv P_{out_{max}}$, corresponds to a high drain efficiency, η_{sat}.

- *Amplifier architecture*: Figure 4.4 also makes it clear that peak drain efficiency η_{sat}, will increase as P_{sat} approaches P_{DC}. From Equation (4.2), we see that an ideal drain

efficiency of 100% is achieved when operating a PA whose $P_{DC} = P_{sat}$, in its saturation region, $P_{out} = P_{sat}$.

Hence, amplifiers which can achieve a peak output power, P_{sat}, that is close to the DC supply power, will yield a high *peak drain efficiency*. Power amplifiers exhibit a fundamental tradeoff between *peak drain efficiency* and *linearity*, and are divided into various classes which represent compromises along this tradeoff.

- *Class-A* PA is characterized by being the most linear, i.e. having the largest linear dynamic range of amplification, but also having the lowest peak drain efficiency, η_{sat}.
- *Class-C* PA is characterized as being among the most non-linear, with very high peak drain efficiency.
- *Class-B* PA provides a compromise between *A* and *C*, being moderate both in linearity and efficiency, and a host of other letter classes exist denoting amplifiers which perform at different points along the linearity-efficiency tradeoff (i.e. *Class-AB* amplifiers which present a compromise between classes *A* and *B*).

The reason for this tradeoff is the *conduction angle* of the PA, or the portion of an RF cycle in which the PA pulls current from the DC supply. *Class-A* amplifiers use their transistors as current sources, and thus always drain current from the DC power line – this corresponds to a conduction angle of 360º. *Class-B* amplifiers are more efficient having a conduction angle of 180º, that is, conduction over ½ of the RF duty cycle. *Class-C* amplifiers do even better with conduction angles of less than 90º. This allows the *Class-C* amplifier to gain significant power savings and use almost all of its DC power supply in amplifying the output. Figure 4.5 graphically describes the linearity-efficiency tradeoff among *Class-C*, *B*, and *A* amplifiers:

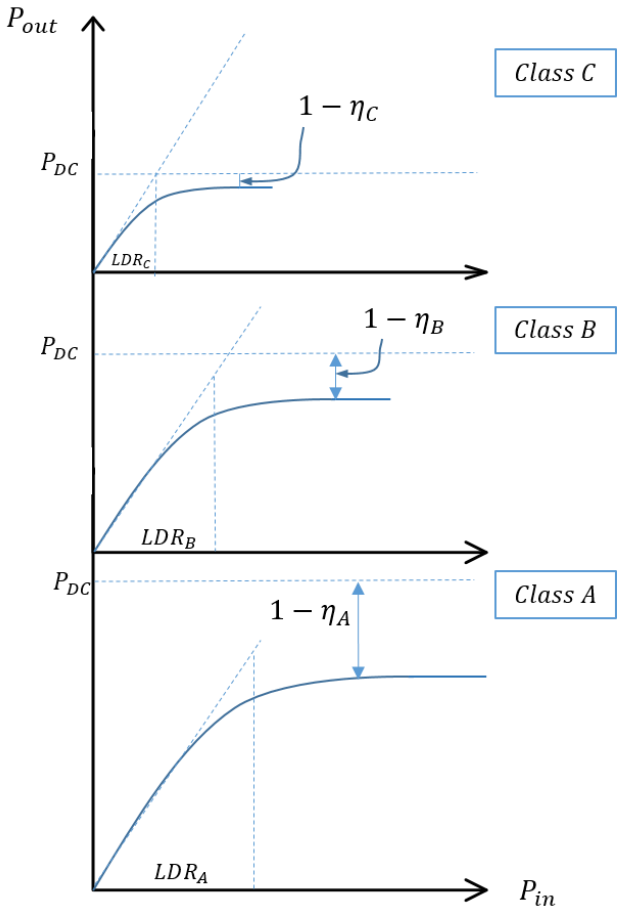

Figure 4.5: Linearity-Efficiency Tradeoff among Class-C, B, and A PAs

4.2.2 OFDM Linearity Requirement

Because OFDM conveys its information through variations in the amplitude, or envelope, of the RF signal, OFDM symbols require linear amplification to faithfully transmit their data. If an OFDM symbol is amplified non-linearly by the PA, its amplitude, and thus its symbol identity, will be distorted.

In general, non-linear amplification of amplitude modulated (AM) signals gives way to a host of undesired signal behaviors including *intermodulation distortion* (IMD). As the input power to a non-linear PA peaks beyond its linear dynamic range, and reaches its *third-order intercept point* (IIP3), the PA will begin amplifying harmonics or *spurs* of the input signal with equal power to fundamental frequencies of the input signal [8]. This harmful result critically corrupts the input signal and significantly expands its spectrum in a phenomena called *spectral regrowth*. OFDM

then faces a critical dilemma. The high PAPR of OFDM demands high PA linearity to avoid suffering these undesirable effects, and this demand for linearity results in a demand for PA power inefficiency. The tradeoff between linearity and inefficiency in amplifying OFDM signals is described in the following subsection.

4.2.2.1 Linearity and Inefficiency

Linearization describes a class of techniques employed to allow a high-PAPR OFDM signal to operate within the linear regime of its PA. The three AM-AM curves of figure 4.6 describe the general approach to linearization required by all OFDM systems, and motivates an understanding of OFDM's need for PA inefficiency:

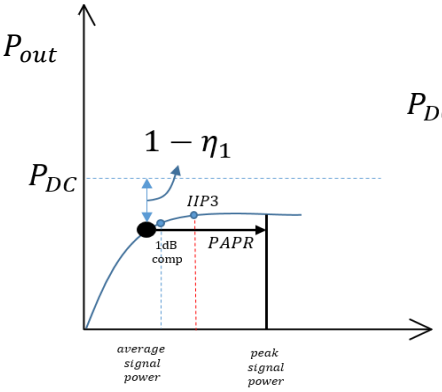

Figure 4.6a: Nonlinear Amplification of OFDM

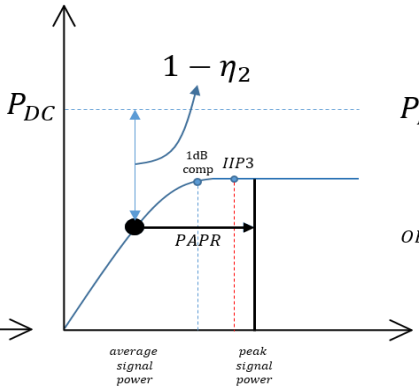

Figure 4.6b Linear Amplification of OFDM

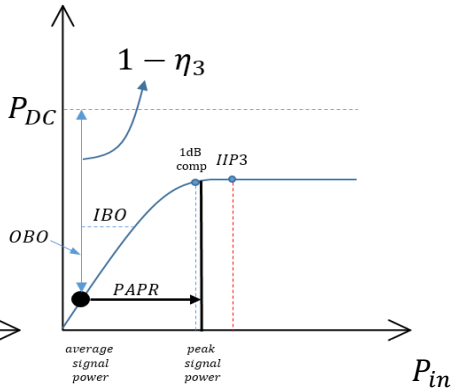

Figure 4.6c: Linear Amplification of OFDM with IBO

Nonlinear Amplification:

The AM-AM curve of Figure 4.6a describes a very efficient, yet entirely impractical, design for amplification of an OFDM signal. Here an efficient, nonlinear PA is used, such that the peak drain efficiency is very good. Also, the average power of the signal is chosen to be within the linear regime (below the 1dB compression point). This is a highly desirable amplifier operation from an efficiency standpoint.

However, the PAPR of the signal, displayed as the range between the average signal power and peak signal power, extends well beyond two points of critical importance on the AM-AM curve–

the 1dB compression point (which governs linear PA operation) and the IIP3 point (which governs spurious free PA operation). Thus, this signal will be irreparably distorted, and will undergo unacceptable spectral regrowth.

Linear Amplification w/o Power Backoff:

The AM-AM curve of Figure 4.6b does slightly better to remedy non-linear PA effects. Operating at the same average power point, the transmitter now employs a PA with greater linearity. A look at the signal PAPR shows that now about half of the PAPR range of the signal will fall within the linear region of the amplifier. While better than the transmitter design in Figure 4.6a, this bodes poorly for the fidelity of the amplitude-modulated symbols. The figure also shows that, in comparison to the amplification in Figure 4.6a, much less of the signal PAPR range will exceed the IIP3 point thus IIP3 distortion affects occur with lower probability.

Linear Amplification with Power Backoff:

The AM-AM curve in Figure 4.6c describes how the issues of Figures 4.6a and 4.6b are remedied in typical OFDM transmitter architectures. The average power of the OFDM signal will be 'backed-off', or attenuated, before amplification to better contain the PAPR of the signal within the linear and spurious free ranges. The level of attenuation is called input-power backoff (IBO) and has a corresponding output-power backoff (OBO) as illustrated in Figure 4.6c. Now, a look at the PAPR of the signal shows that the signal will no longer operate within the IIP3 range of the PA, avoiding the harmful effects of intermodulation distortion and spectral regrowth, and will be amplified linearly, i.e. within the 1dB compression point, over the close to the full range of the input signal.

Figure 4.6c describes the general *linearization* approach required for power amplification of OFDM signals. While it does well to achieve desired linearity, we see just how badly the average drain efficiency of the PA, denoted by η_3, suffers. Nearly all of the power provided by the PA DC supply is wasted and dissipated as heat as only a small fraction is actually used to amplify the signal. Without the use of added linearization technologies, OFDM will require drain efficiency of less than 20% [6]!

4.2.2.2 Additional Linearization Techniques

The technique used in Figure 4.6c to maintain linearity was the input-power backoff (IBO) approach. Note that backing off the input signal power does not reduce the PAPR of the signal, but merely pushes the average power point lower on the AM-AM curve. It is clear that if the PAPR of the signal can be reduced, the amount of IBO required to achieve linearity can also be reduced along with the IBO drain efficiency penalty. A number of *PAPR Reduction* techniques exist including PAPR reduction coding, tone reservation, and clipping. While these can be effective in reducing the PAPR of the OFDM signal, they will incur some combination of *additional overhead*, *signal distortion*, and *added complexity* to the system and still cannot remedy the inefficiency inherently required by the highly-linear PA.

Hardware Linearization techniques exist in the form of additional circuitry, before and/or after the PA in the RF chain, that helps to provide an aggregate transfer curve with an extended linear regime. Such hardware linearization technologies include digital predistortion, feedback and feedforward linearization, Envelope Elimination and Restoration (EER), and Linear Amplification with Nonlinear Components (LINC) [8]. These methods work to varying levels of success in the task of extending linearization while maintaining PA efficiency, however they can be quite complex, distorting, and in practice can very rarely enable linear amplification of OFDM with an average drain efficiency of 40% (60% power waste).

4.3 Power Consumption Considerations

Power efficiency is a very important consideration in all technologies, and certainly in communication systems. Today's smartphones may come equipped with high performance CPUs and intricate displays, but the vast majority, over 60%, of their power consumption is consumed by the RF system-on-a-chip (SoC) processor [4], upwards of 70% of which goes specifically toward powering the various onboard PAs. In cellular base stations, upwards of 80% of power consumed is used for the task of power amplification [6].

The fact that OFDM will require 80% of this power to be wasted is a startling thought for a very OFDM-driven wireless world. This affects consumers by demanding shorter battery lives of their mobile devices, and cellular network carriers by demanding very high power supply to their base station PAs. It has been estimated that cellular network providers spend over $36B annually on

powering their base stations [10]. Moreover, the communications industry is responsible for roughly 10% of the global energy consumption and carbon footprint, and the environmental impact of the wastefulness of OFDM PAs . As we continue to envision a world with greater wireless connectivity, capacity, and throughput, it behooves us to consider optimally power-efficient approaches to address the OFDM PAPR problem.

5 CONSTANT-ENVELOPE OFDM

The previous chapters have covered OFDM, considering the merits which have made it such an important technology and also the PAPR problem which makes OFDM systems suffer large power wastage. The OFDM PAPR problem can be summarized by the following: *The inherently large PAPR of OFDM demands highly linear power amplification, and by rule-of-thumb highly linear power amplification is equivalent to highly inefficient power amplification*. PAPR-reduction techniques seek to reduce the power backoff required by OFDM before amplification, and hardware linearization techniques seek to extend the linear operation regime of the power amplifier, but to totally cure its power inefficiency woes, OFDM needs to be cured of the need for highly linear amplification and RF processing. This is the motivation for the constant envelope OFDM (CE-OFDM) waveform.

5.1 CE-OFDM Concept

CE-OFDM provides a highly intriguing solution to the PAPR-reduction problem. It takes the high-PAPR OFDM signal and modulates the phase rather than the amplitude of the RF carrier. The passband RF signal will thus have a constant amplitude, or a constant-envelope. The figure 5.1 graphically represents the effect of phase modulation on the complex envelope of the OFDM signal.

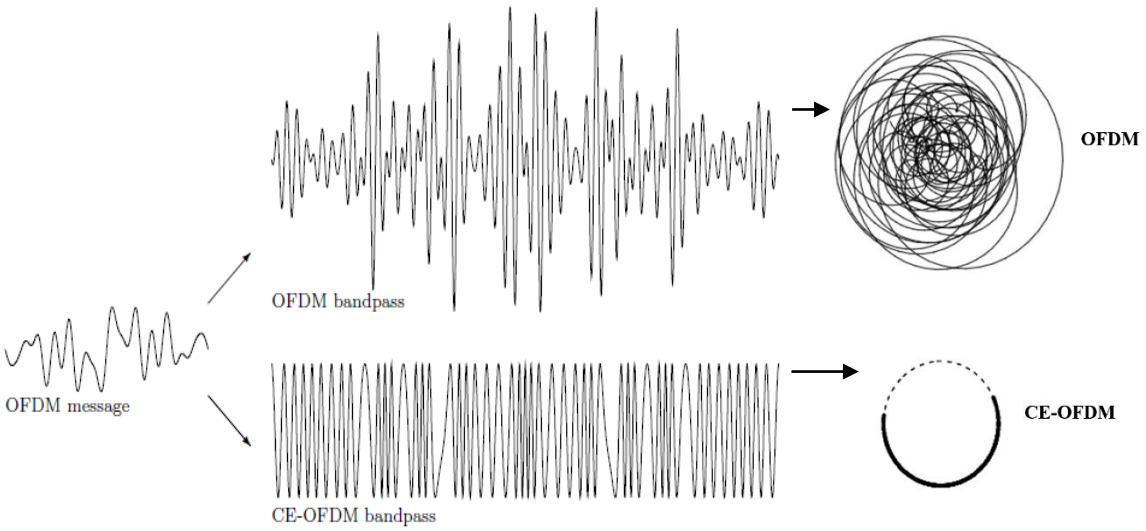

Figure 5.1: CE-OFDM Envelope vs. OFDM Envelope

Figure 5.2 displays the instantaneous power of an OFDM signal against that of a CE-OFDM signal over one symbol interval.

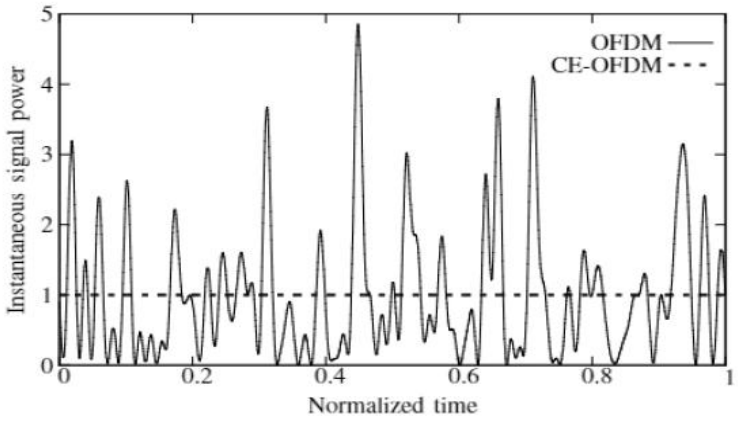

Figure 5.2: Instantaneous Power of CE-OFDM vs OFDM

The instaneous power of a CE-OFDM signal will always be constant, meaning its peak power will be equal to its average power - PAPR of 0dB. This completely eliminates the need for linear amplification, promising a substantial increase in power efficiency of OFDM systems. This is one of several highly intriguing properties of the CE-OFDM waveform. To begin a discussion of these properties, the following subsection begins an analytic description of the waveform.

5.2 CE-OFDM Signal Definition

To begin an analytical description of a CE-OFDM signal, consider how a standard OFDM signal is modulated from baseband to passband. Recall the expression of a baseband OFDM waveform:

$$m(t) = \sum_{i} \sum_{k=0}^{N-1} I_{i,k} e^{j\frac{2\pi kt}{T_s}} \; g(t - iT_s) \tag{5.1}$$

The notation $m(t)$, denotes that this signal will be used as the *message* signal component phase modulator. A general expression for the baseband CE-OFDM waveform $s(t)$ is yielded when the signal $m(t)$ modulates the phase of a complex exponential, resulting in the following constant envelope signal:

$$s(t) = e^{jm(t)} \tag{5.2}$$

$m(t)$ is called the *message* or *phase signal* of the CE-OFDM waveform. A CE-OFDM receiver is tasked with extracting the message signal from the phase of the constant envelope signal. Because

the argument of a complex phasor must be a real, $m(t)$ in expression (5.2) must be a purely real signal. This requires that symbol set, $\{I_{i,k}\}$, in $m(t)$ must also be purely real; that is, the message signal of CE-OFDM can support only real-valued data symbols - those on a 1-dimensional constellation. The implications of the latter are further considered in the performance analysis section.

After passband modulation, the general CE-OFDM passband expression of (5.1) results:

$$\begin{aligned} y(t) &= Re\{s(t) \cdot e^{j\omega_c t}\} \\ &= Re\{e^{j(\omega_c t + m(t))}\} \\ &= \cos(\omega_c t + m(t)) \end{aligned} \tag{5.3}$$

Again, note the CE-OFDM passband waveform is a phase modulation with a message of an OFDM signal $m(t)$. A simplified block diagram for the transmitter and receiver of the baseband CE-OFDM signal is expressed in Figure 5.3. This general block diagram of the CE-OFDM receiver and transmitter introduces only two new blocks, for phase modulation and demodulation, to the OFDM system.

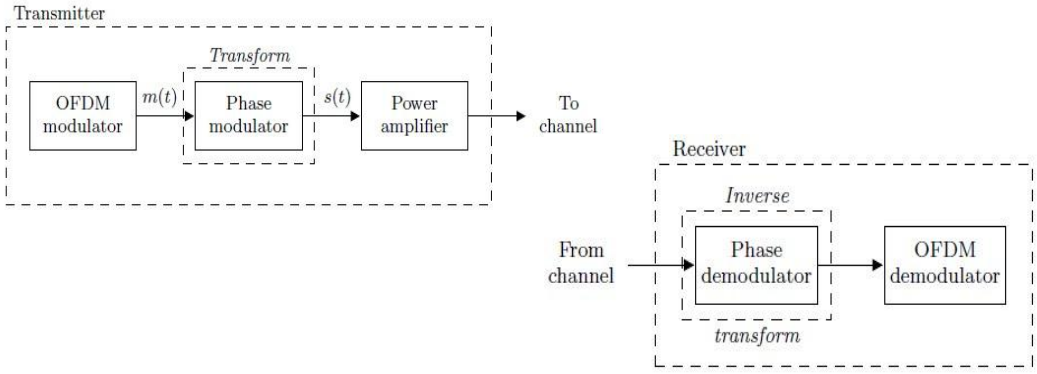

Figure 5.3: Simplified CE-OFDM Block Diagram

The CE-OFDM signal (5.2) is largely defined by its message signal. One important condition on $m(t)$ has been mentioned, which is that phase modulation of this signal requires that the message signal must be purely real. A formal definition of the CE-OFDM message signal expresses this and other important conditions and considerations of the waveform, as well as its fundamental parameters.

5.3 CE-OFDM Waveform Parameters

The OFDM message signal $m(t)$ for a CE-OFDM waveform is formally defined as follows:

$$m(t) = 2\pi h C_n \sum_{i} \sum_{k=0}^{N-1} I_{i,k} q_k[t - iT_s] + \theta_i \qquad (5.4)$$

This expression remains consistent with the general form of expression (5.1) with a few new terms. Each of the terms in this expression describe some important signal parameters for the CE-OFDM waveform. These are expressed in the subsections that follow [18][11-13].

5.3.1 Symbol Mapping $\{I_{i,k}\}$:

$\{I_{i,k}\}$ in (5.4) is the set of the N symbol values which modulate the N OFDM subcarriers on the i^{th} symbol interval. Because $m(t)$ must be real to be used for phase modulation, its symbol values $\{I_{i,k}\}$ must also be real, and thus mapped to a 1-dimensional constellation. For independent and equally likely symbols, M-ary pulse-amplitude modulation (PAM) becomes the optimum symbol mapping. Accordingly, the symbols $\{I_{i,k}\}$ must be chosen from the set:

$$I_{i,k} \in \{-M + 1, -M + 3, \ldots, -1, 1, \ldots, M - 3, M - 1\}$$

where M is the constellation size of the PAM modulation.

5.3.2 Subcarrier Set $\{q_k(t)\}$:

$\{q_k(t)\}$ in (5.4) is the set of orthogonal subcarriers. The selection of a subcarrier set in $m(t)$ becomes critical. Two CE-OFDM specific constraints must be considered in the choice of subcarrier. The first of these is that the subcarriers must be purely real signals. As defined in (2.3), standard IFFT-based OFDM uses complex subcarriers. The real-valued restriction of $m(t)$ means that real-valued subcarriers must be used. The most natural choices of real-valued subcarrier sets $\{q_k(t)\}$ are perhaps the following sinusoidal signal sets:

Sine-wave subcarriers:

$$q_k(t) = \begin{cases} \cos(p\pi k \Delta f t), & 0 \le t < T_s = 1/\Delta f \\ 0, & o.w. \end{cases} \quad k = 0, \ldots, N-1$$

Cosine-wave subcarriers:

$$q_k(t) = \begin{cases} \sin(p\pi k\Delta f t), & 0 \le t < T_s = 1/\Delta f \\ 0, & o.w. \end{cases} \quad k = 0, \ldots, N-1 \tag{5.6}$$

which both satisfy the orthogonality property:

$$\int_0^T q_i(t) q_j(t) dt = \begin{cases} \varepsilon_{sub}, & (i = j) \\ 0, & (i \neq j) \end{cases} \quad k = 0, \ldots, N \tag{5.7}$$

The variable p in the subcarrier expressions scales the nominal bandwidth value of $\{q_k(t)\}$ with respect to that of the complex subcarrier set $\{e^{j2\pi k\Delta f t}\}$. When $p = 1$, the nominal bandwidth of the sinusoids $\{q_k(t)\}$ and $\{e^{j2\pi k\Delta f t}\}$ are equal, but $\{q_k(t)\}$ will have half the subcarrier spacing, and each will be a harmonic of a half period sinusoid [11][18].

A judicious choice of $\{q_k(t)\}$ is necessary in the design of the CE-OFDM system. A decided advantage of the sine-wave set comes from the property that each subcarrier $q_m(t)$ in the set approaches 0 at the symbol boundaries ($as, t \to T_s \; and \; t \to 0+$). From (5.4), $m(t)$ amounts to a linear summation of these subcarriers, so this property enforces $m(t)$ always being continuous across symbol boundaries. Making $m(t)$ continuous provides a valuable gain in spectral containment, which is desired to counter the spectral efficiency disadvantages of its real-valued constraint. Figure 5.4 depicts the OFDM signal with both cosine and sine wave subcarriers, with the sine-wave subcarriers displaying continuity over symbol boundaries.

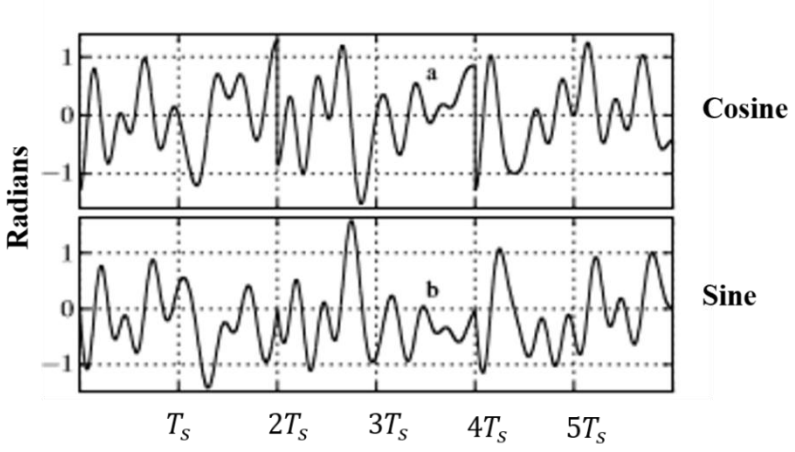

Figure 5.4: Inter-Symbol Continuity for Sine and Cosine Subcarriers

The scaling of p in (5.5) and (5.6) corresponds to scaling of the signal bandwidth, and in applications with generous bandwidth allotment, bandwidth expansion may prove desirable as the

phase modulated subcarrier symbols will be spread over a wider bandwidth providing the signal greater frequency diversity.

5.3.3 Normalization Constant C_n:

C_n in (5.4) is a normalization constant which normalizes the variance of the modulated subcarriers on the right-hand side of the expression. The variance, σ_d, for equally-likely independent symbols from an M-ary PAM constellation is given by $\sigma_d = \frac{M^2-1}{3}$. The expression for C_n is then given by:

$$C_n = \sqrt{\frac{2}{N\sigma_d^2}} = \frac{3}{M^2-1}\sqrt{\frac{2}{N}} \tag{5.8}$$

5.3.4 Modulation Index $2\pi h$:

The normalization constant C_n allows the modulation index h in Equation (5.4) to scale the variance of the message signal, and the outer 2π coefficient converts this value into radians.
Increasing the value of h increases the symbol energy in the message signal $m(t)$, and correspondingly increases the Euclidean distance between the message symbols. Because the expression in the double summation in Equation (5.4) is normalized by the constant C_n, regardless of the modulation order of $I_{i,k}$, increasing the modulation index becomes necessary in order to increase the Euclidean distance of the message symbols to accommodate higher order modulations. The modulation index is a very important parameter of a CE-OFDM waveform, the choice of which, as discussed in Section 5.5, has critical implications regarding both error-rate performance and spectral containment of the CE-OFDM signal.

5.3.5 Memory Phases θ_i:

Memory phases, θ_i, in (5.4) are optional terms. These are constant phase offsets added to each CE-OFDM symbol group in order to ensure continuous phase across symbol boundaries. The values chosen for these memory phases are defined in Section 5.4.

5.4 CE-OFDM Discrete-Domain Processing

With the message signal completely defined, (5.2) shows that the baseband CE-OFDM waveform is computed by making this message the argument of a complex phasor. This is the last step strictly necessary before multiplying by the carrier and transmitting, but to bolster the resistance of the signal to multipath fading it is desirable to add a cyclic prefix to each symbol. Cyclic prefixing is performed in the digital domain on discrete samples of $s(t)$. At a sampling rate of f_s, and a sampling period $t_s = 1/f_s$, the discrete digital CE-OFDM baseband signal, $s[n]$, is given by:

$$s[n] = s(nt_s) = e^{jm(nt_s)} \tag{5.9}$$

A full symbol period of the message OFDM signal occurs every $N = f_s T_s$ samples. Cyclic prefixing entails taking the final L samples of each symbol and appending them to the beginning of that symbol, and generates a new baseband CE-OFDM sequence $s'[n]$. The new symbols will have a length $N' = N + L$, and thus a longer symbol duration $T_s' = (L + N)t_s$. The prefixed CE-OFDM sequence $s'[n]$ now has an underlying OFDM message sequence $m'[n] = \arg(s'[n])$. The addition of cyclic prefixes reintroduces discontinuity at the symbol boundaries. Figure 5.5 shows the effect of cyclic-prefixing on the underlying message signal.

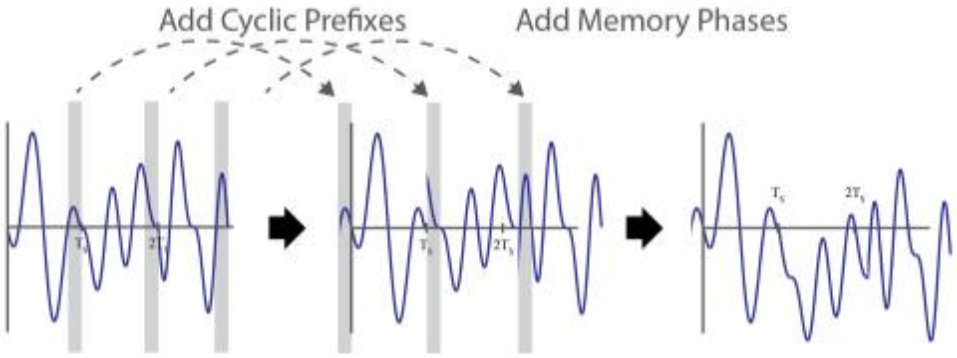

Figure 5.5: Memory Phase Continuity after Cyclic Prefixing

Figure 5.5 shows that if a judiciously chosen memory phase constants θ_i are added to each symbol, the message signal $m(t)$ will be made continuous across symbol boundaries. This is the purpose of θ_i, in Equation (5.4). A simple recursion rule for calculating the proper values of these memory phases, θ_i, to add to the signal message signal $m(nt_s)$ to negate the discontinuity in $s'(nt_s)$ is presented below:

$$\theta_i = \begin{cases} -m((N-L)t_s), & i = 0 \\ -m\big((kN-L)t_s\big) + \sum_{i'=0}^{i-1} \theta_{i'}, & i > 0 \end{cases} \tag{5.10}$$

With these memory phases added to the message signal (5.4), the discrete baseband CE-OFDM signal (3.10), can be cyclic-prefixed and retain its continuity. A DAC converts this discrete digital signal to a continuous analog waveform, which is then mixed with a high frequency carrier to generate the passband CE-OFDM waveform from (5.3). A block diagram of the CE-OFDM transmitter is displayed in Figure 5.6.

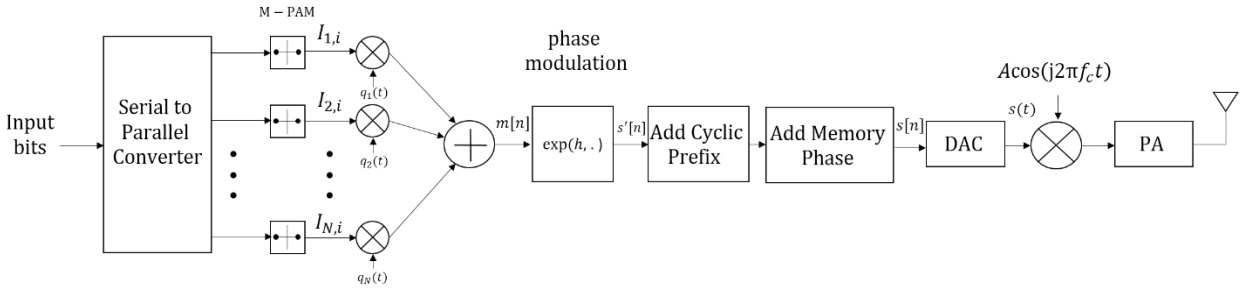

Figure 5.6: CE-OFDM Transmitter Block Diagram

With the CE-OFDM waveform now analytically defined, Section 5.5 begins an analysis of spectral and error performance of the waveform. As considered in Section 5.3, there are a number of the component parameters of CE-OFM. For this reason, a performance discussion of CE-OFDM is not simple task. The goal of the next section is to facilitate this discussion.

5.5 CE-OFDM Performance Consideration

Two immediate performance questions come to mind when considering CE-OFDM: how does the phase modulation affect the spectrum of the signal, and how well does the signal perform in the presence of noise over an RF channel? Due to the nonlinearity of the modulation, and all of its performance-affecting parameters, these questions are difficult to answer strictly analytically, but some analytical approximations lay a foundation for understanding the performance characteristics

of the waveform. The following subsections use results of the literature [12,13] in analyzing the spectral performance, and the performance of the suboptimal CE-OFDM receiver in AWGN.

5.5.1 Spectral Analysis

The expression for the effective bandwidth of the CE-OFDM waveform is developed by using the following Taylor series expansion,

$$e^x = \sum_{n=0}^{\infty} \frac{x^n}{n!} \tag{5.10}$$

to approximate the baseband CE-OFDM, $s(t)$,

$$\begin{aligned} s(t) &= Ae^{jm(t)} \\ &\approx A\sum_{n=0}^{\infty}\left[\frac{j^n m^n(t)}{n!}\right] \end{aligned} \tag{5.11}$$

the effective double-sided bandwidth (or the nominal bandwidth), W, of the $n = 1$ term of the summation can be defined as twice the highest frequency subcarrier within the message signal $m(t)$. From the discussion in Section 5.3.2, when $p = 1$ or half wave subcarriers are used, this yields a nominal bandwidth:

$$W = 2 \cdot \left(\frac{N}{2T_s}\right) = \frac{N}{T_s} \tag{5.12}$$

This corresponds to an approximation of the lower bound of the nominal bandwidth of $s(t)$, as the $n = 2$ term in the Taylor series will have a nominal bandwidth of $2W$, etc. The actual bandwidth of the CE-OFDM signal will be dependent upon the parameters of its modulation, specifically the choice of modulation index h, but empirical measurements of fractional-out-of-band power (FOBP) show W to be a good approximation for the effective signal bandwidth. Figure 5.7 displays estimated curves of the Welch power spectral density (PSD), of a $N = 64$ CE-OFDM waveform at multiple values of h, in terms of the FOBP:

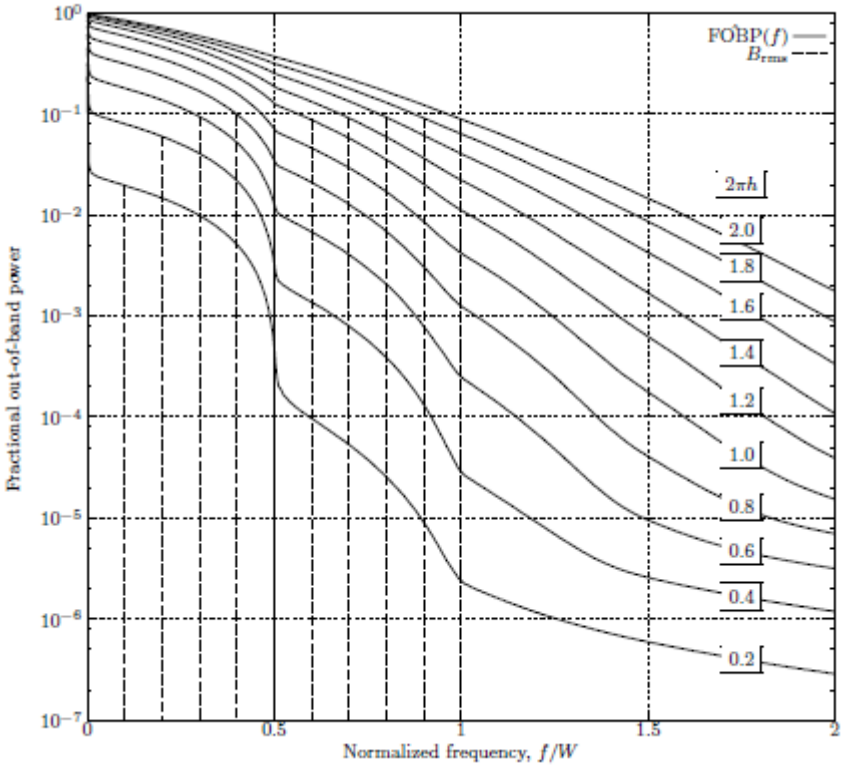

Figure 5.7: CE-OFDM Power Spectral Density Estimate FOBP

The PSD estimate curves in Figure 5.7 show that, for all values of h from 0.2 to 2.0 radians, over 90% of total signal power is contained within the nominal bandwidth $f = W$. A general property of phase modulated signals is also observed in that tuning the modulation index tunes the spectral containment of the signal. Decreasing h has the effect of reducing the signal bandwidth, while increasing h has the effect of spreading the signal bandwidth. The following subsection considers the error performance of a sub-optimal CE-OFDM receiver and will express how the choice of h presents a fundamental tradeoff between signal bandwidth and error performance in CE-OFDM.

5.5.2 The Sub-Optimal CE-OFDM Receiver

The receiver shown Figure 5.8 provides a block diagram for the suboptimal CE-OFDM receiver.

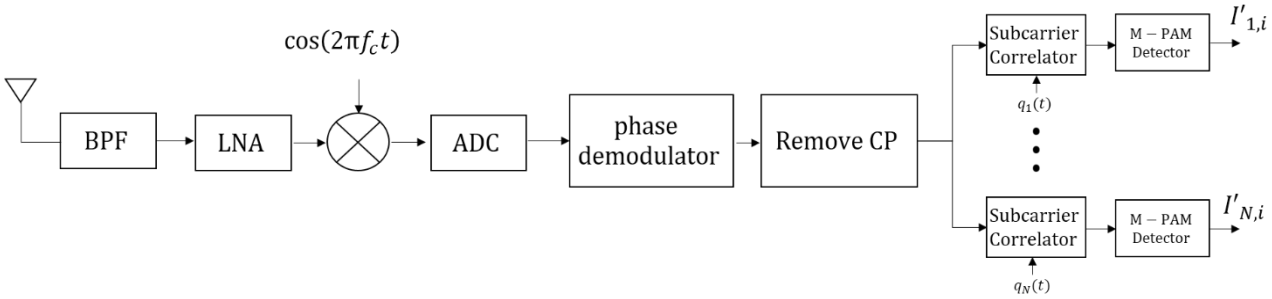

Figure 5.8: Suboptimal CE-OFDM Receiver Block Diagram

This receiver architecture uses a *phase demodulator* to extract the phase from the CE-OFDM signal, and retrieve the OFDM message signal. After discarding the cyclic prefix samples on each symbol duration, subcarrier correlation is performed to make a nearest Euclidean-distance decision on the transmitted M-ary modulation symbol on each subcarrier.

The most significant task of the receiver is the phase demodulation, and it is important to understand the effect of this nonlinear operation on the performance of the receiver. The theoretical performance of a receiver in AWGN provides a basis for characterizing the performance of a waveform over noisy RF channels, and the following subsection develops an analytical approximation for the error probability of the suboptimal receiver of Figure 5.8

5.5.2.1 Theoretical Performance in AWGN

After being received from the AWGN channel and downconverted to baseband, the received CE-OFDM signal is given as,

$$r(t) = s(t)e^{j\phi_0} + n(t) \tag{5.13}$$

where ϕ_0 is a phase offset term, and $n(t)$ is a zero-mean Gaussian random process with a constant double-sided power spectral density of $N_0/2$, for $|f| \leq W/2$. This signal is input to the phase demodulator which yields the following output,

$$\widehat{m}(t) = m(t) + \phi_0 + \xi(t) \tag{5.14}$$

where $m(t)$ is the original OFDM message signal, ϕ_0 is some constant phase offset, and $\xi(t)$ is the phase component of the noise signal $n(t)$. If the carrier signal $Acos(2\pi f_c t)$ has an average signal power A^2 such that $A^2 \gg N_0$, the phase demodulator output noise $\xi(t)$ will be approximately linearly related with $n(t)$ and can be modeled as a zero-mean Gaussian noise process with a power spectral density $\Phi_\xi(f)$ given by,

$$\Phi_\xi(f) = N_0/A^2, \quad \text{for } |f| \leq W/2 \tag{5.15}$$

This result, in which the carrier-to-noise ratio (CNR) of the phase demodulator can be modeled as linearly related with the signal-to-noise ratio (SNR) of the demodulator output, is called the high CNR approximation.

The phase demodulator output $\hat{m}(t)$ becomes the input to the bank of N subcarrier correlators, the output of each of which, taken over the symbol duration T_s, is given by,

$$\begin{aligned} Q_k &= \int_0^{T_s} \hat{m}(t) q_k(t) dt \\ &= \int_0^{T_s} \{m(t) + \phi_0 + \xi(t)\} q_k(t) dt \\ &\equiv S_k + \Psi_k + N_k \end{aligned} \tag{5.16}$$

which says that the output of the kth subcarrier correlator will be composed of a message signal component, S_k, a phase offset component, Ψ_k, and a phase noise component, N_k, which are defined by,

$$\begin{aligned} S_k &= \int_0^{T_s} m(t) q_k(t) dt \\ &= \int_0^{T_s} \left\{ 2\pi h C_n \sum_{k'=1}^{N} I_{k'} q_{k'}(t) + \theta_i \right\} q_k(t) dt \\ &= \int_0^{T_s} 2\pi h C_N \sum_{k'=1}^{N} I_{k'} q_k(t) q_{k'}(t)\, dt \\ &= 2\pi h C_n I_k * \left(\frac{T_s}{2}\right) \\ &= 2\pi h \sqrt{(1/2) N \sigma_d^2}\ \cdot I_k \end{aligned} \tag{5.17}$$

$$\Psi_k = \int_0^{T_s} \phi_0 q_k(t) dt = 0 \qquad (5.18)$$

$$N_k = \int_0^{T_s} \xi(t) q_k(t) dt \qquad (5.19)$$

where N_k, the $q_k(t)$ component of the Gaussian noise process $\xi(t)$, becomes a zero-mean Gaussian random variable with a variance, $VAR[N_k] \simeq \frac{1}{2T} N_0/A^2$, which is the frequency component of $\xi(t)$ at $f = f_k$, the k_{th} subcarrier frequency. The result is that the subcarrier correlator output Q_k is now given by,

$$Q_k = 2\pi h \sqrt{(1/2) N \sigma_d^2} \cdot I_k + N_k \qquad (5.20)$$

which is an M-ary PAM symbol with a zero-mean Gaussian noise term. Using the Maximum Likelihood (ML) rule, and the relationship that $\sigma_d^2 = (M^2 - 1)/3$ for equally likely i.i.d M-ary PAM symbols, the symbol error probability of the receiver is given as [13]:

$$P_s(e)_{CE-OFDM} \simeq 2\left(\frac{M-1}{M}\right) \cdot Q\left(2\pi h \sqrt{\frac{6 \log_2 M}{M^2 - 1} (E_b/N_0)}\right) \qquad (5.21)$$

Due to the placement of the modulation index as the coefficient of the argument within the Q-function, the modulation index is a very powerful parameter which can significantly tune the symbol error performance of the CE-OFDM signal. Figure 5.9 displays plots of the symbol error performance of an 8-PAM CE-OFDM waveform over a range of modulation index.

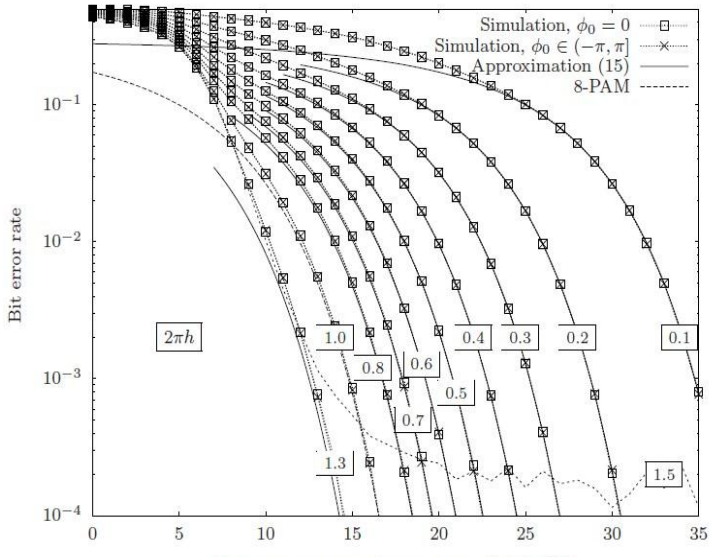

Figure 5.9: CE-OFDM Symbol Error Rate vs SNR vs various $2\pi h$

5.6 Critical Performance and Design Considerations

The brief analytical discussions of CE-OFDM spectral and error-rate performance provide a foundation for understanding much of the character of the waveform. In this section a point-by-point discussion of some of these traits is provided. The following subsection summarizes some of the key challenges in the design of CE-OFDM systems and the subsequent subsection summarizes the various merits of the CE-OFDM waveform.

5.6.1 The Challenges of CE-OFDM

While the result of Equation (5.21) describes the ideal error-rate performance of CE-OFDM, a few practical considerations will make the performance deviate from this. One assumption made in the derivation from Equation (5.14) is that the phase demodulator is able to recover a perfect copy of the message signal with some additive noise interference term. The following subsections present various factors which impact the performance of CE-OFDM, and challenge CE-OFDM design.

5.6.1.1 Phase Demodulation Challenges

One of the general philosophies of CE-OFDM is offloading the task of handling the high-PAPR signal from the PA, to the phase demodulator in the CE-OFDM receiver. An OFDM signal with very pronounced variations in amplitude, becomes a constant envelope signal which will have very pronounced variations in phase. This means that the receiver phase demodulator must be capable of tracking these phase variations. Spectrally-efficient message signals (i.e. with a large number of subcarriers and/or large modulation index) will have high PAPR and thus cause the phase of the CE-OFDM signal to make intermittently large excursions along the unit circle of the constant envelope carrier. This phenomenon is visualized in Figure 5.10:

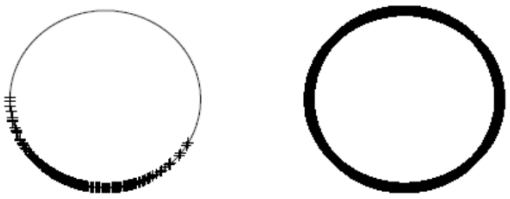

Figure 5.10: Phase Excursions of CE-OFDM vs *h*

In Figure 5.10 the complex amplitude of a CE-OFDM signal is plotted along the unit-circle over multiple samples. It is shown that the CE-OFDM signal with the higher value of modulation index h will make wider excursions along the unit-circle of the carrier. Because the message signal $m(t)$ is normalized by the constant C_n, regardless of its modulation order, it becomes necessary to increase the value of h to properly scale the Euclidean distance to accommodate higher order modulations. For this reason, it is helpful to associate higher values of h with higher-PAPR, higher-order message signals.

Figure 5.10, illustrates the difficulty of the task that the phase demodulator can have in tracking the phase of a high h signal. Because phases take on values only in the range $(-\pi, +\pi]$, the phase demodulator must determine when the information-carrying phase makes 'wraps' around the phase value boundaries and reconstruct the correct amplitude of the message signal.

One simple method to address this challenge is called the *phase unwrapping* algorithm. The phase unwrapping algorithm works by simply taking the phase argument of consecutive complex samples of the signal, and if the two phases differ by more than π radians, then the algorithm

determines that the phase has ‘wrapped’ over a phase boundary and ‘unwraps’ this by adding $\pm\pi$ radians to the next sample.

The phase unwrapping algorithm expects that the phase of the signal will make gentle excursions along the unit-circle and thus will be very effective for signals with low h and high SNR. However, signals with high h and/or high phase noise will commonly make wide swings in phase along the unit-circle, and if these swings are greater than π radians over one sampling interval then the unwrapper algorithm will make ‘false wrap’ errors, which will cause degraded performance. The false wrap errors of the phase unwrapper can be reduced with the use of high oversampling value, such that the sampling interval is small enough to track very fast excursions of the phase, and also employing appropriate filtering to remove any out-of-band noise components before the task of phase demodulation. More advanced techniques for phase tracking are possible with some added complexity. These include phase-locked-loop (PLL) and cyclic-slip estimation (CSE) [22].

5.6.1.2 The FM Threshold Problem

Angle modulation, whether FM or PM, experiences the phenomenon called *FM thresholding*. When the CNR of the angle-modulated CE-OFDM signal drops below 10 dB, the linear relationship between the CNR of the received signal and the SNR at the output of the phase demodulator fails, resulting in an increase in phase noise which will cause the message signal to become critically obscured by phase noise. Below the FM threshold, the phase demodulator will not be able to properly track the highly unstable phase, resulting in phase demodulator error, and the message signal, even if correctly extracted, becomes too obscured by error to decode. Techniques to extend the FM threshold range exist [22], but CE-OFDM system designers should be careful to avoid operation below 10 dB CNR in order to aid phase tracking and message signal detection in the phase demodulator receiver.

5.6.1.3 Real Message Signal Requirement

As discussed in Section 5.3.2, the phase modulator message signal is required to be purely real, and this requires the CE-OFDM subcarriers to be purely real. For this reason, twice the number of subcarriers, with half the subcarrier separation, is required for CE-OFDM to provide the same nominal bandwidth as OFDM. In the context of multicarrier communications, condensing subcarrier separation naturally raises some concerns regarding maintaining subcarrier

orthogonality, but as is discussed in the strengths section to come, this concern is mitigated in CE-OFDM. The more poignant issue with the real-message signal requirement is that it constrains subcarrier modulations to be of the 1-dimensional, M-ary PAM variety which certainly restricts the spectral efficiency of CE-OFDM in comparison to OFDM, whose subcarriers can be modulated by any symbols on a 2-dimensonial constellation.

5.6.1.4 Multiple Access and Standards Integration

One challenging engineering problem will be the integration of CE-OFDM waveforms into present OFDM-based standards. The linearity and subcarrier orthogonality of OFDM which enables the OFDMA multiple access scheme is no longer present in CE-OFDM. For instance, two users transmitting CE-OFDM simultaneously in a channel would incur interference on each other regardless of which message signal subcarriers were modulated. This means that traditional forms of single-carrier multiple access techniques may be required for CE-OFDM systems, a restriction which diverges from the trend of next generation wireless communications. Some intelligent engineering would be required to adapt CE-OFDM into the next generation standards.

5.6.2 The Strengths of CE-OFDM

CE-OFDM is a single-carrier modulation scheme which takes on much of the nature of a multi-carrier modulation scheme. The modulation scheme transmits symbols in parallel over a wideband channel, but it does so on a single carrier. The phase modulation can then be considered as a non-linear spreading or ‘smearing’ of the multicarrier signal, which is recovered by the phase demodulator. In this way, CE-OFDM retains the critical characteristics of a multicarrier signal, with a few additional benefits:

5.6.2.1 ISI-Immunity

As described in Section 5.4, the addition of a cyclic prefix to a CE-OFDM symbol block has the identical purpose and effect as in standard OFDM. With small overhead in symbol time to a long duration CE-OFDM symbol, the cyclic prefix effectively mitigates ISI. Like OFDM, CE-OFDM requires only simple equalization and can make use of single-carrier frequency-domain equalization (SC-FDE) techniques.

5.6.2.2 Multipath Diversity Gain

Another interesting characteristic of CE-OFDM found in the literature [21], is that the phase modulation 'spreading' of the OFDM signal results in an enhanced layer of resistance to the effects of multipath channel fading. The OFDM subcarriers are effectively spread about in frequency, and the phase demodulator inherently yields some multipath diversity gain in multipath rich channels.

5.6.2.3 Carrier Recovery

The OFDM message signal in CE-OFDM is modulated on the phase of an RF carrier, and because of this, the challenge of maintaining subcarrier orthogonality is effectively eliminated. For this reason, CE-OFDM systems will require simpler frequency synchronization requirements.
Also, Equations (5.17) and (5.19), in the receiver performance derivation show that constant phase offset terms drop out of the subcarrier correlator output. As a result, with a high quality phase demodulator, the signal can be non-coherently demodulated.

5.6.2.4 Flexible Waveform Parameterization

The many performance tuning knobs of the CE-OFDM waveform make it very interesting to study, and a strong candidate for use in adaptive or cognitive radio communications. The modulation index h in particular is a highly influential parameter which can tune signal performance, trading off signal bandwidth and error rate performance.

5.7 Nonlinear Power Amplification of CE-OFDM

The greatest benefit of CE-OFDM is its ability to be amplified nonlinearly. The AM-AM curves in Figures 5.11a and b provide a visualization of the contrast in PA efficiency of an OFDM system and a CE-OFDM system.

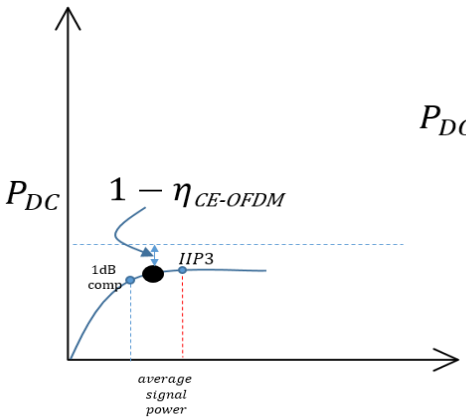

Figure 5.11a: Class C Nonlinear Amplification of CE-OFDM

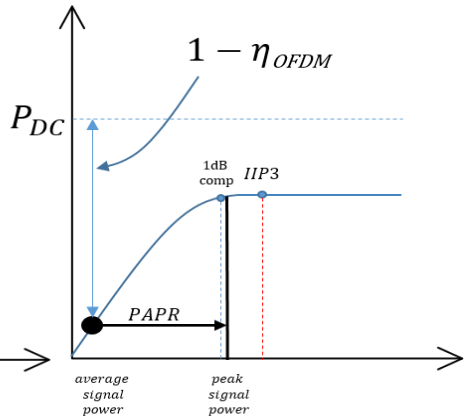

Figure 5.11b: Class A Linear Amplification of OFDM

Figure 5.11a shows that the use of cheap and highly-efficient switched-mode amplifiers (i.e. Class C and D) allow CE-OFDM signals to be amplified at near saturation to yield drain efficiency approaching 90% [15,20]. CE-OFDM promises the reality of broadband mobile systems with the PA efficiency of GMSK-based 2G systems and this is proof positive that the waveform should be very seriously considered and developed in research and industry for the next generations of wireless communications standards. The following chapter in this thesis presents a software-defined radio system designed to enable rapid-prototyping, off-line or adaptive reconfiguration, and testing of the CE-OFDM systems.

6 SDR IMPLEMENTATION OF CE-OFDM WAVEFORM

The CE-OFDM waveform has been presented in the previous chapter as a novel technique for optimal PAPR reduction in OFDM systems. The waveform has a number of interesting properties and performance-affecting parameters. To study these, an SDR implementation of a rapid-prototypable CE-OFDM system has been adopted. Details of the GNU Radio SDR development framework are presented in Section 1, and Sections 6.2 and 6.3 of detail the software implementation of the CE-OFDM transmitter and receiver.

6.1 GNU Radio SDR Development

GNU Radio is an open-source, highly extensible software framework for developing SDR applications and waveforms on a GPP. The key components of the GNU Radio software framework are defined in the subsections that follow:

6.1.1 Signal Processing Blocks

In GNU Radio, signal processing blocks are modular structures, written in C++ or Python, which use signal processing algorithms to process digital signal samples. Signal processing blocks are the fundamental components of waveforms. Source and sink blocks form the bookends of a GNU Radio 'flowgraph'.

Source blocks are signal processing blocks which have outputs but no inputs, and generate the samples of a digital signal at the input of the GNU Radio waveform. *Software source blocks* use software routines to generate and stream digital signal samples into the GNU Radio waveform. *Hardware source blocks* set up hardware drivers or network sockets to stream digital signal samples from hardware sources such as computer soundcards, UDP or TCP network applications, and RF front ends such as USRPs, into the GNU Radio waveform.

Sink blocks are signal processing blocks that have inputs but no outputs. They consume digital samples at the output of the GNU Radio waveform. *Software sink blocks* in GNU Radio include a number of graphical user interface (GUI) modules which provide a graphical display of

input data samples. *Hardware sink blocks* use hardware drivers or network sockets to stream digital signal samples out of GNU Radio waveforms and into hardware devices.

6.1.2 GNU Radio Scheduler

The GNU Radio Scheduler is the heart of the GNU Radio system. When a flowgraph is executing, the GNU Radio Scheduler buffers and cycles digital samples into and out of each block in the waveform, enabling the GPP to perform real-time baseband modulation and demodulation.

6.1.3 Python Programmatic Interface

The primary interface to the GNU Radio framework is the Python language. Python provides a clean and simple interface to the GNU Radio system and abstracts away details of memory management from the programmer. Once GNU Radio libraries are imported, all GNU Radio blocks become accessible in Python. This allows a programmer to implement GNU Radio flowgraphs by instantiating all blocks in the flowgraph, by connecting them in a 'top block' object. When the 'run' method of the top block object is called, the GNU Radio scheduler will begin real-time processing of the user-defined flowgraph.

6.1.4 GNU Radio Companion Graphical Interface

GNU Radio also provides a graphical user interface (GUI), called GNU Radio Companion (GRC) to accompany its Python programmatic interface. In GRC the user can instantiate GNU Radio blocks graphically by dragging and dropping graphical blocks onto a workspace and chaining them together to form a flowgraph. Upon execution of the graphical flowgraph, an underlying Python script is generated and executed to begin real-time processing of the flowgraph.

6.1.5 Creating Custom GNU Radio Blocks

The extensibility of the GNU Radio system is founded on the object-oriented programming (OOP) principle of inheritance. In the inheritance principle, one object, called a child, *inherits* the attributes of another object, called a parent. Custom blocks or modules in GNU Radio inherit a software structure as illustrated in Figure 6.1.

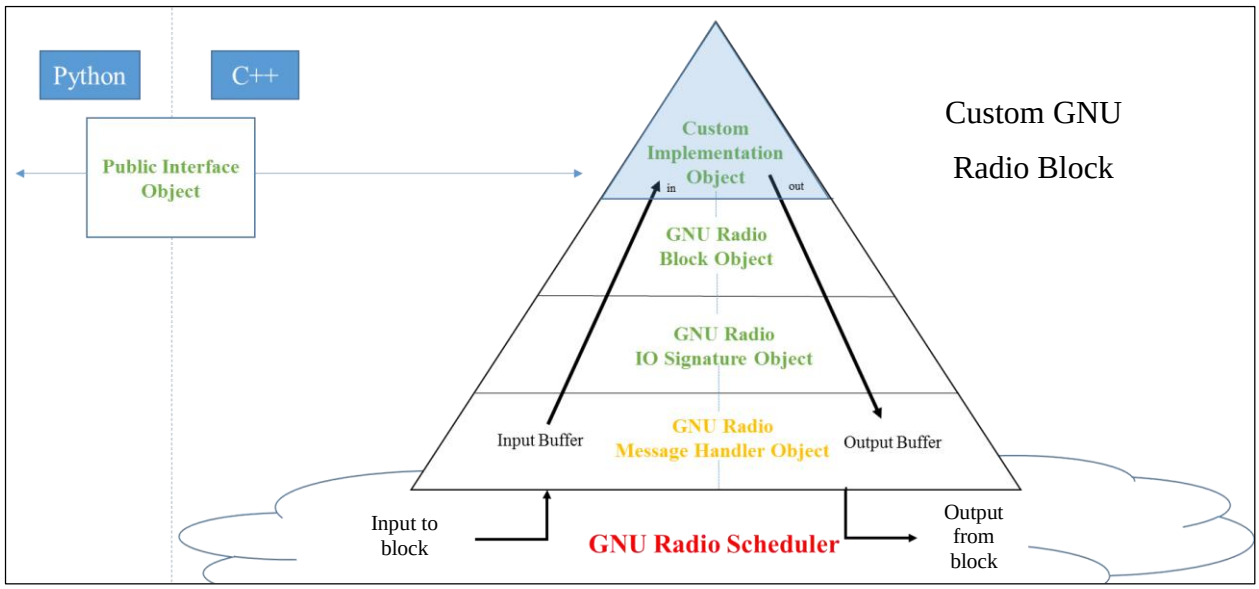

Figure 6.1: GNU Radio Block Inheritance

In Figure 6.1, the inheritance principle of a GNU Radio C++ signal processing block is represented as a pyramid, where each layer of the pyramid represents an object defined in the GNU Radio framework. The top layer in the pyramid is the user-defined *'Implementation Object'*. This object contains the 'work' method of the block, in which the user defines a custom signal processing algorithm which processes the samples of a digital signal. When called, this function takes samples which are inputted to the block from the GNU Radio scheduler, processes them, and returns output samples back out to the GNU Radio scheduler to be passed into another block in the flowgraph. As shown in Figure 6.1, the implementation object inherits the functionality of a GNU Radio *'Block Object'*. The block object inherits a GNU Radio *'IO Signature Object'*. The IO signature object defines the number of inputs and outputs of the block, as well as the data type of each item in the input and output streams. The IO signature object then inherits a GNU Radio *'Message Handler Object'* which handles the buffering of data samples passed into and out of the work function of the implementation object of the block.

The last object of a custom GNU Radio block is the *'Public Interface Object'*. As displayed in Figure 6.1, this object is not a part of the inheritance structure of the block, but it performs critical tasks in the system. The public interface block contains a constructor which instantiates the full block – the implementation object and its full inheritance – and returns a pointer to the

implementation object. The public interface object then uses the Python Simplified Wrapper and Interface Generator (SWIG) to make the block importable and accessible in Python. For example, via SWIG a Python script is able to import the C++ defined block, and call the block constructor of the public interface, and pass in any variables required to define the block functionality.

GNU Radio developers have provided a helpful command line utility called 'gr_modtool'. This command line utility creates the directory system of the custom block, edits all makefiles, and generates a variety of source code templates for defining and customizing various objects which compose the custom block structure.

The implementation of the CE-OFDM waveform of this thesis is composed of several custom GNU Radio blocks and is detailed in Sections 6.2 and 6.3.

6.2 CE-OFDM Transmitter Implementation

The CE-OFDM transmitter is implemented in GNU Radio as a Python 'source' block. Blocks written in Python have the same inheritance structure described in Figure 6.1, but does not need a *public interface object* because they are readily importable in Python. All component objects and methods of the transmitter waveform are defined and implemented in a single script *CEOFDM_TX.py*. Figure 6.2 shows the GRC graphical interface of the CE-OFDM transmitter block.

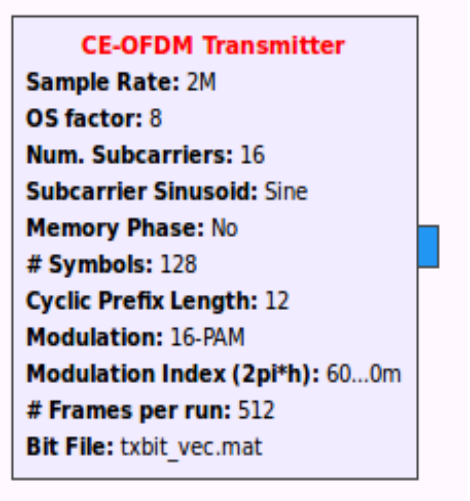

Figure 6.2: Graphical Interface of CE-OFDM Transmitter Block

The parameters of the transmitter block allow the user to customize the modulation of the CE-OFDM waveform by defining the *number of subcarriers N*, *PAM modulation order M*, *modulation index* $2\pi h$, the *choice of sine or cosine subcarriers*, and the *choice of applying memory phases* across symbol boundaries.

The interface of the transmitter block also includes parameters such as *sample rate*, *oversampling factor*, *cyclic prefix length (in samples)*, and *number of symbols per frame*, which allows the user to customize the time dimensions of a transmission frame. The structure of a transmission frame created by the CE-OFDM Transmitter block is displayed in Figure 6.3.

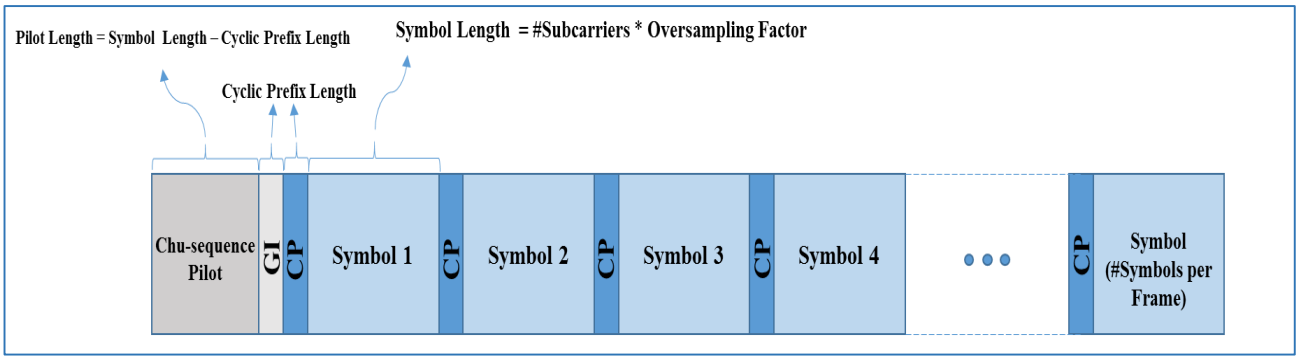

Figure 6.3: Transmitter Frame Structure Diagram

Figure 6.3 details how the parameter interface of the transmitter block enables the user to customize the frame structure of the CE-OFDM waveform. The *oversampling factor* multiplied by the *number of subcarriers* yields the length in samples of each CE-OFDM symbol, or the oversampling rate of the waveform. The *cyclic prefix length* is the number of samples to be prepended from the end to the beginning of each symbol. After generating the specified *number of symbols per frame* the transmitter block prepends the consecutive symbols and cyclic prefixes with a Zadoff-Chu sequence pilot which is used for time synchronization at the receiver. The pilot is followed by a guard interval of the same length in samples as the cyclic prefix. The length of the pilot is chosen such that the pilot and the guard interval occupy the same interval as one symbol. In the current implementation, the transmitter block is strictly a 'source' block. This means the transmitter block generates output samples but takes no inputs. The data that the transmitter block modulates are passed into the block through a binary file, via its *'Bit File'* parameter. The transmitter reads the bits of the file and follows the signal processing stages as shown in Figure

5.6 to generate CE-OFDM baseband symbols. The interface of the block also contains a parameter for the *number of frames transmitted per run*. The transmitter will transmit this number of frames, each frame separated by one cyclic prefix interval, before stopping the transmitter flowgraph.

6.3 CE-OFDM Receiver Implementation

The CE-OFDM receiver implementation is a hierarchical block, composed of a mixture of custom and pre-existing GNU Radio blocks. In Figure 6.4 the hierarchical diagram for the receiver of a 6 subcarrier, 16-PAM CE-OFDM waveform is displayed.

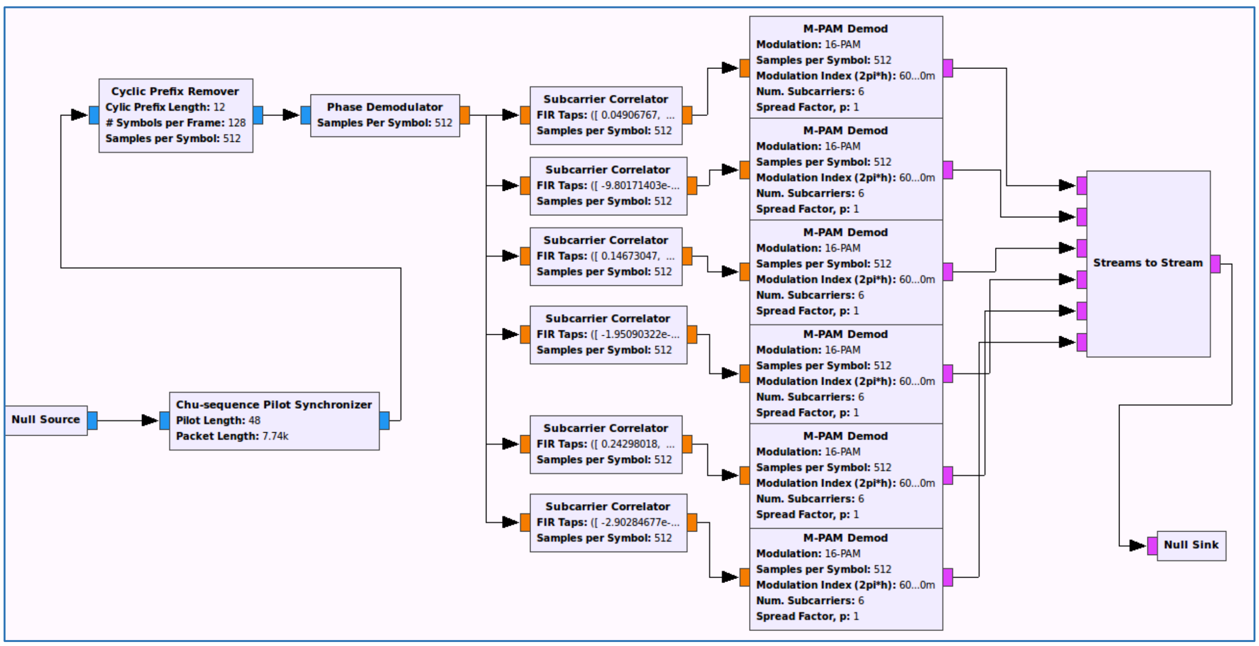

Figure 6.4: Hierarchical Diagram of CE-OFDM Receiver

The blocks which compose the receiver in Figure 6.4, follow closely the blocks of the suboptimal receiver structure of Figure 5.8. Disregarding the *Null Source* and *Null Sink* placeholders at the bookends of the flowgraph, the composite blocks of the CE-OFDM receiver are described as follows:

- The *'Chu-Sequence Pilot Synchronizer'* block performs timing synchronization of a CE-OFDM frame. It is a hierarchical Python block, composed of a number of C++ blocks

which perform the tasks of correlating the input signal with the known Chu-sequence pilot, normalizing the correlator output and applying a threshold to determine when the beginning of a frame has been synchronized. The pilot synchronizer block prevents any samples from passing into the flowgraph until synchronization is detected.

- The *'Cyclic Prefix Remover'* block is a custom C++ block that discards the cyclic prefix samples at the beginning of each symbol in the frame.
- The *'Phase Demodulator'* block is custom C++ block that extracts the message signal from the phase of the CE-OFDM baseband signal. The phase demodulator first takes the argument of the input samples and attempts to accurately reconstruct the message signal by unwrapping the signal from the $[-\pi, \pi)$ domain to $\mathbb{R}$.
- The *'Subcarrier Correlator'* block is a hierarchical Python block which uses a GNU Radio FIR filter object to convolve a message symbol with the *k*th subcarrier.
- The *'M-PAM Demodulator'* block is a custom C++ block which scales the subcarrier correlator outputs onto an *M*-ary PAM constellation, and performs a maximum-likelihood estimate of the transmitted PAM symbol amplitude, and uses a Gray-code mapping to output a corresponding symbol value.

The final block in the system is the *'Streams to Stream'* block, a GNU Radio block that performs parallel-to-serial conversion of the received symbols. The graphical interface of the CE-OFDM receiver block is displayed in Figure 6.5.

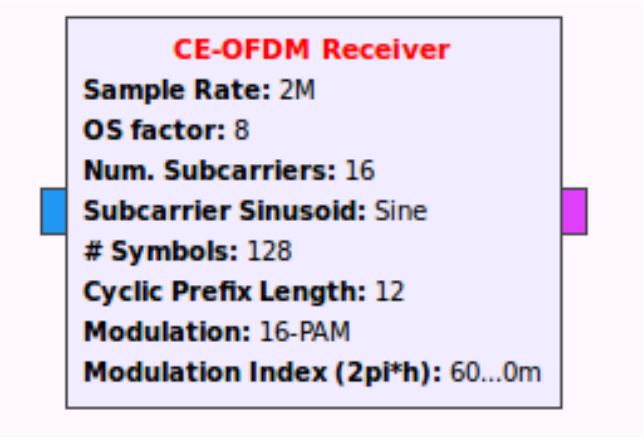

Figure 6.5: Graphical Interface of CE-OFDM Receiver

7 SIMULATION METHODOLOGY ANDD RESULTSS

This chapter describes the methodology for testing the performance of the GNU Radio CE-OFDM waveform, and presents the results of these simulations.

7.1 Simulation Methodology

Figure 7.1 displays a GNU Radio *simulation flowgraph* constructed to test the performance of the CE-OFDM receiver described in Section 6.4, in an AWGN channel. The simulation flowgraph contains two new custom GNU Radio blocks, namely the *'AWGN Block'* and the *'CE-OFDM BER Block'*.

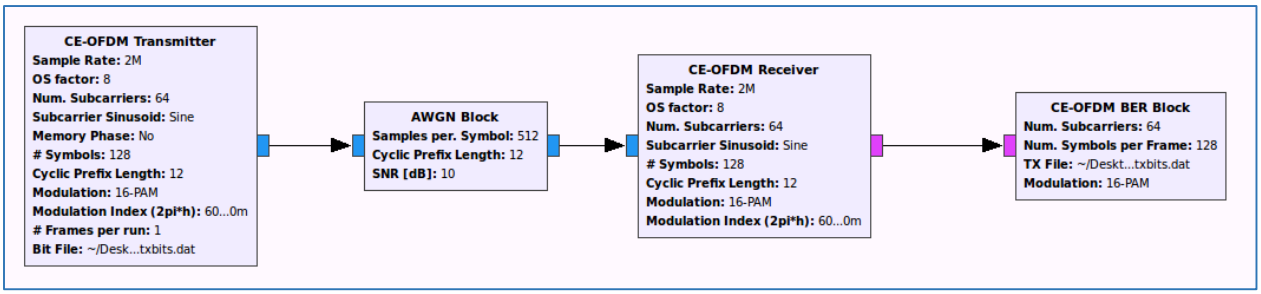

Figure 7.1: GNU Radio Simulation Flowgraph

The AWGN block is a hierarchical block which generates a vector of zero-mean Gaussian noise samples to add to each symbol and cyclic prefix interval of an input CE-OFDM sample stream. As represented in the expression of the baseband CE-OFDM signal in Equation (5.2), the samples of a CE-OFDM symbol will be a phasor with unit amplitude. Correspondingly the root-mean-squared (rms) amplitude of the CE-OFDM symbols is unity. The AWGN block uses the expression in Equation (7.2) to determine the rms amplitude of the Gaussian noise signal to add to each symbol.

$$SNR_{\mathrm{dB}} = 20\log\left(\frac{S_{rms}}{N_{rms}}\right) \tag{7.1}$$

where S_{rms} is the unity rms amplitude of the signal, and N_{rms} is the rms amplitude of the noise,

$$N_{rms} = \frac{S_{rms}}{10^{\left(\frac{SNR_{\mathrm{dB}}}{20}\right)}} = 10^{-\left(\frac{SNR_{\mathrm{dB}}}{20}\right)} \tag{7.2}$$

The AWGN block utilizes the GNU Radio *'Gaussian Noise Source'* block to generate a Gaussian noise with the rms amplitude given in Equation (7.2), for a value of signal-to-noise ratio (SNR) specified at the interface of the AWGN block.

The output of the AWGN block in Figure 7.1 is a noisy CE-OFDM signal which is input to the CE-OFDM receiver. The final block in the simulation flowgraph is the CE-OFDM BER block, which receives the demodulated symbols from the CE-OFDM receiver and reads the same binary file from which the transmitter modulates its frames, to calculate the bit-error rate (BER) performance of the system.

The flowgraph in Figure 7.1 is the graphical representation of a GNU Radio *'top block'* object which forms a 'testbench' for testing the CE-OFDM waveform. The testbench is coded with interface parameters to allow the user to configure various parameters of the waveform, the noise level of the AWGN channel, simulate the transmission and reception of 1 million bits CE-OFDM frames, and retrieve the bit error rate (BER) results of the simulation. Figure 7.2 displays an excerpt of Python script which will execute the testbench object over multiple *noise levels of the AWGN channel* and multiple configurations of the *modulation index*, *number of subcarriers*, and *M*-ary *PAM modulation order* of the CE-OFDM waveform.

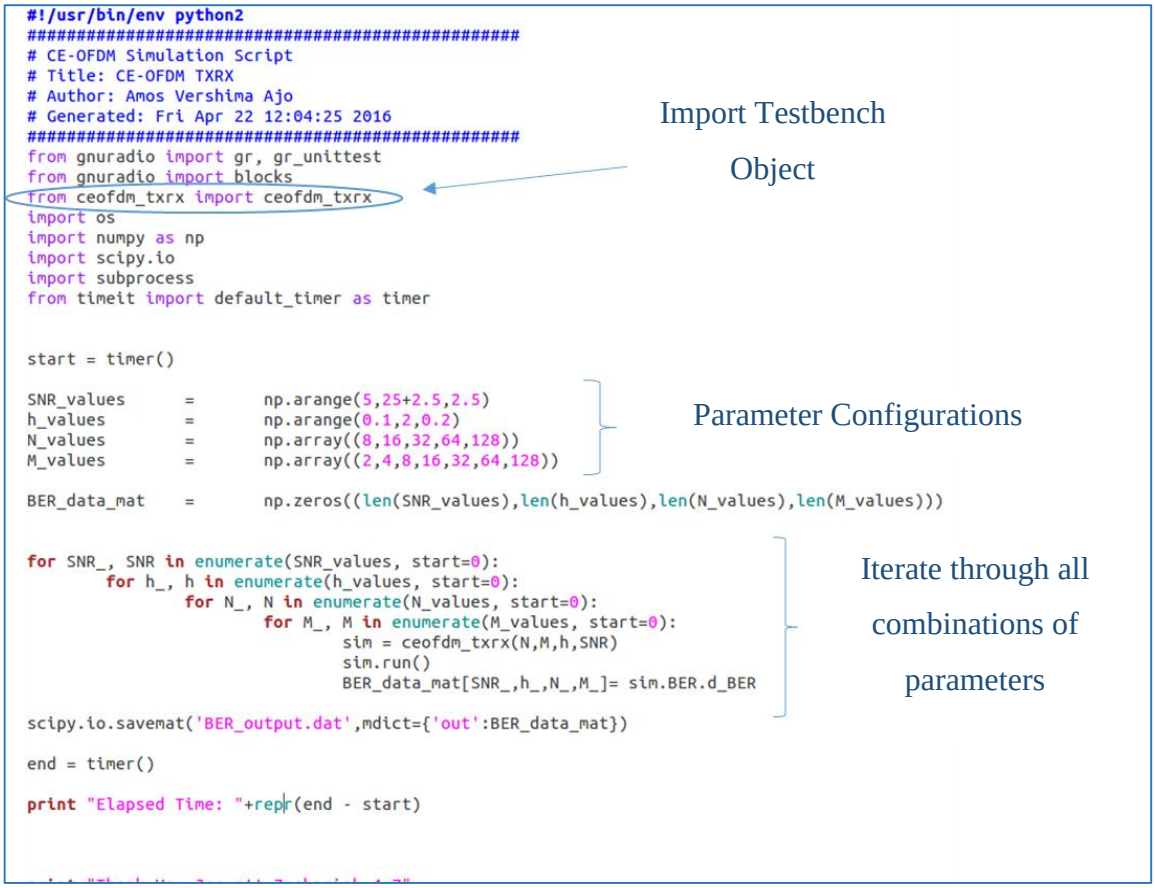

Figure 7.2: Python CE-OFDM Simulation Excerpt

The script in Figure 7.2 yields a 4-dimensional matrix of BER values, for multiple combinations of the above-mentioned parameters. Section 7.2 displays various plots retrieved from this simulation.

7.2 Simulation Results

The Figures 7.3 through 7.6 display BER versus SNR waterfall curves over multiple modulation indices. The simulated curves are plotted against curves derived from the theoretical symbol error rate approximation of the sub-optimal CE-OFDM receiver in AWGN from Equation (5.21).

$$P_s(e)_{CE-OFDM} \simeq 2\left(\frac{M-1}{M}\right) \cdot Q\left(2\pi h \sqrt{\frac{6\log_2 M}{M^2-1}(E_b/N_0)}\right) \qquad (5.21)$$

With Gray-coding, the theoretical BER is given by $P_b(e) \simeq P_s(e)/\log_2 M$.

$$P_b(e)_{CE-OFDM} \simeq 2\left(\frac{M-1}{M\log_2 M}\right)\cdot Q\left(2\pi h\sqrt{\frac{6\log_2 M}{M^2-1}(E_b/N_0)}\right) \tag{7.3}$$

Because the simulation methodology described in Section 7.1 adds a noise signal to the baseband CE-OFDM waveform, the SNR derived in Equation (7.1) is equivalent to the carrier-to-noise ratio. The relationship between the carrier-to-noise ratio and the bit-energy to noise ratio E_b/N_0 of Equation (7.3) is given as follows [13]:

$$E_b/N_0 = (\text{oversampling factor})\cdot SNR/(\log_2 M) \tag{7.4}$$

Hence, the following theoretical BER expression enables comparison with the results of the AWGN simulation.

$$P_b(e)_{CE-OFDM} \simeq 2\left(\frac{M-1}{M\log_2 M}\right)\cdot Q\left(2\pi h\sqrt{\frac{6\cdot SNR\cdot(\text{oversampling factor})}{M^2-1}}\right) \tag{7.3}$$

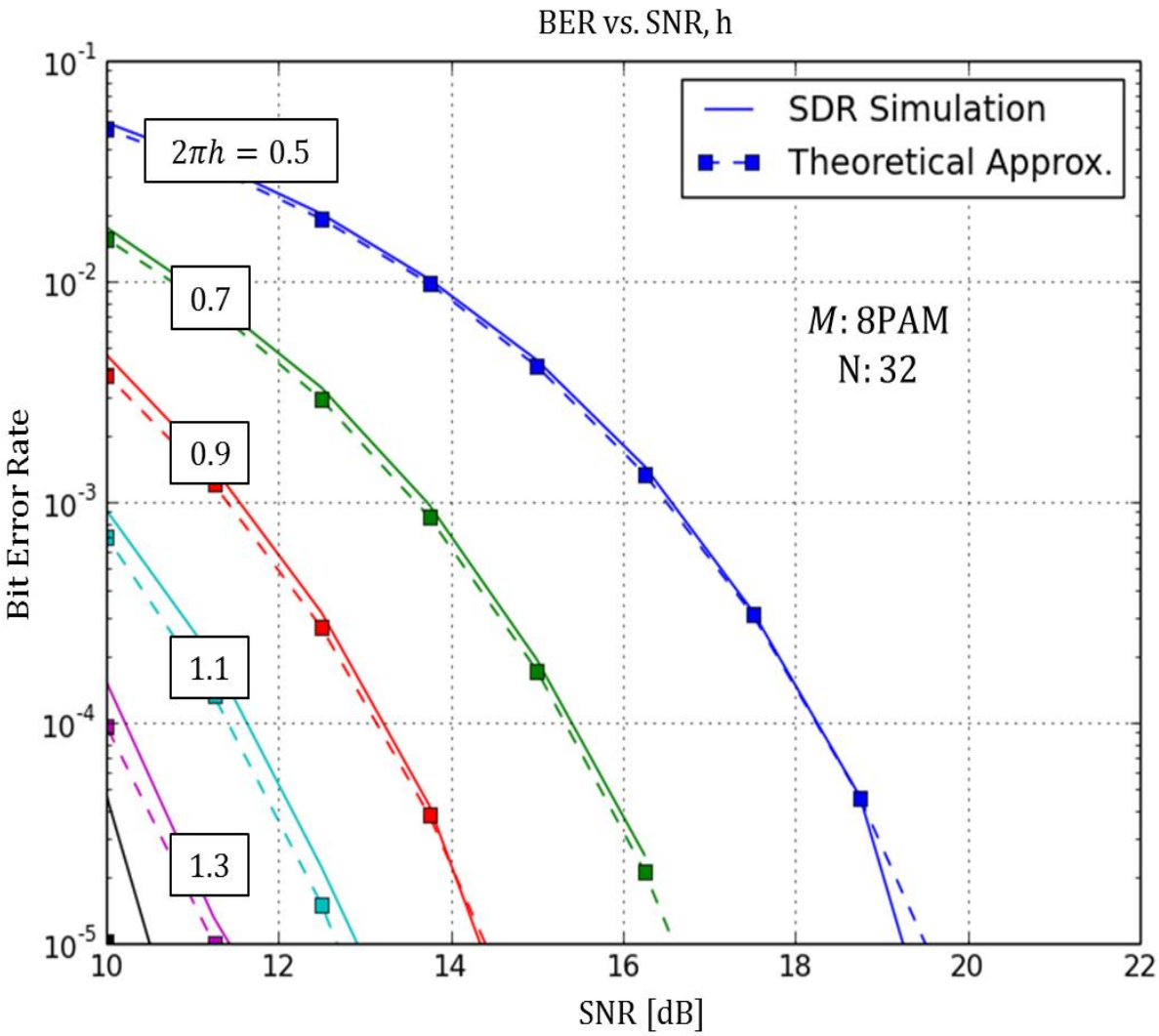

Figure 7.3: 8-PAM, N=32, os factor=8

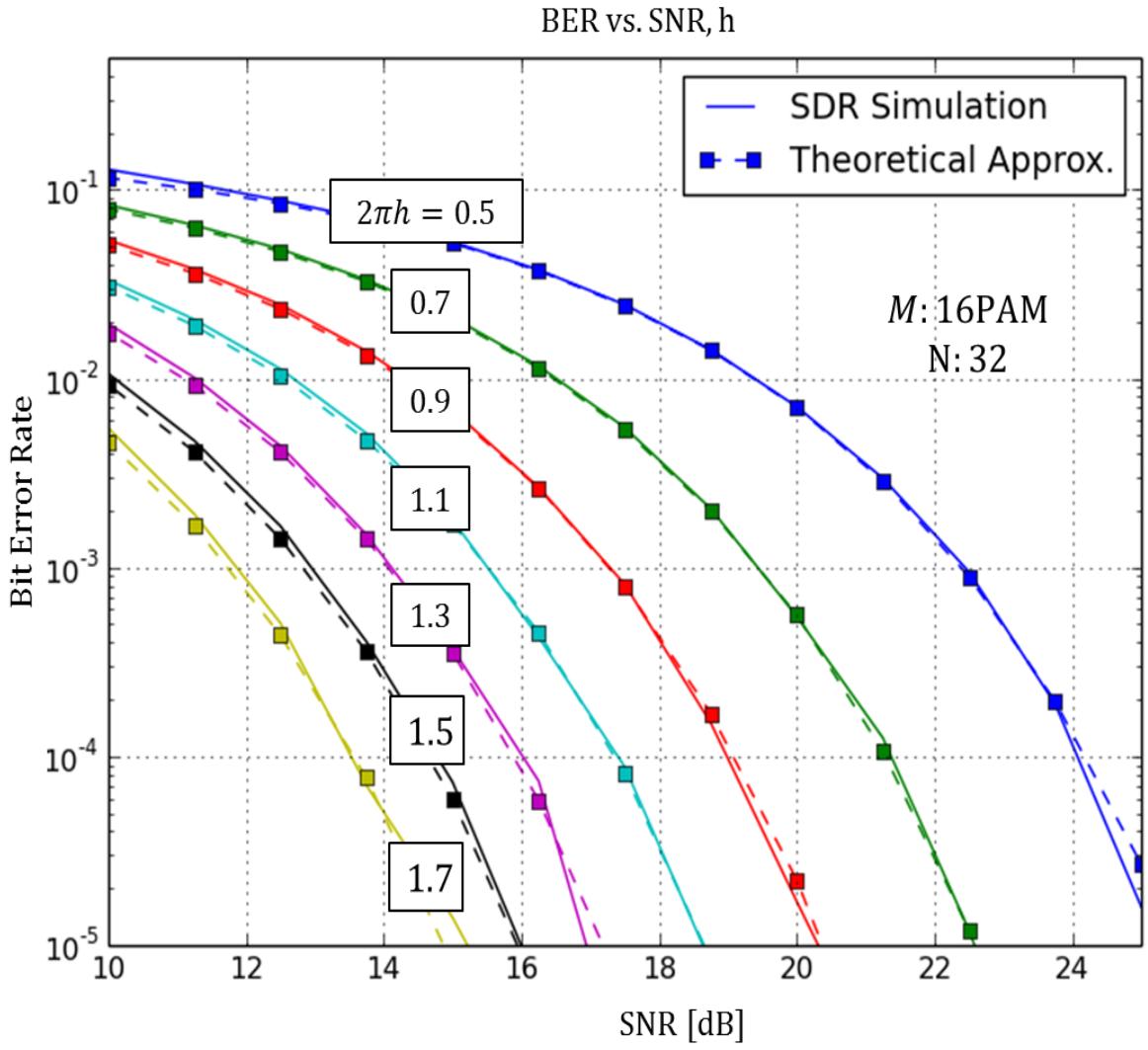

Figure 7.4: 16-PAM, N=32, os factor=8

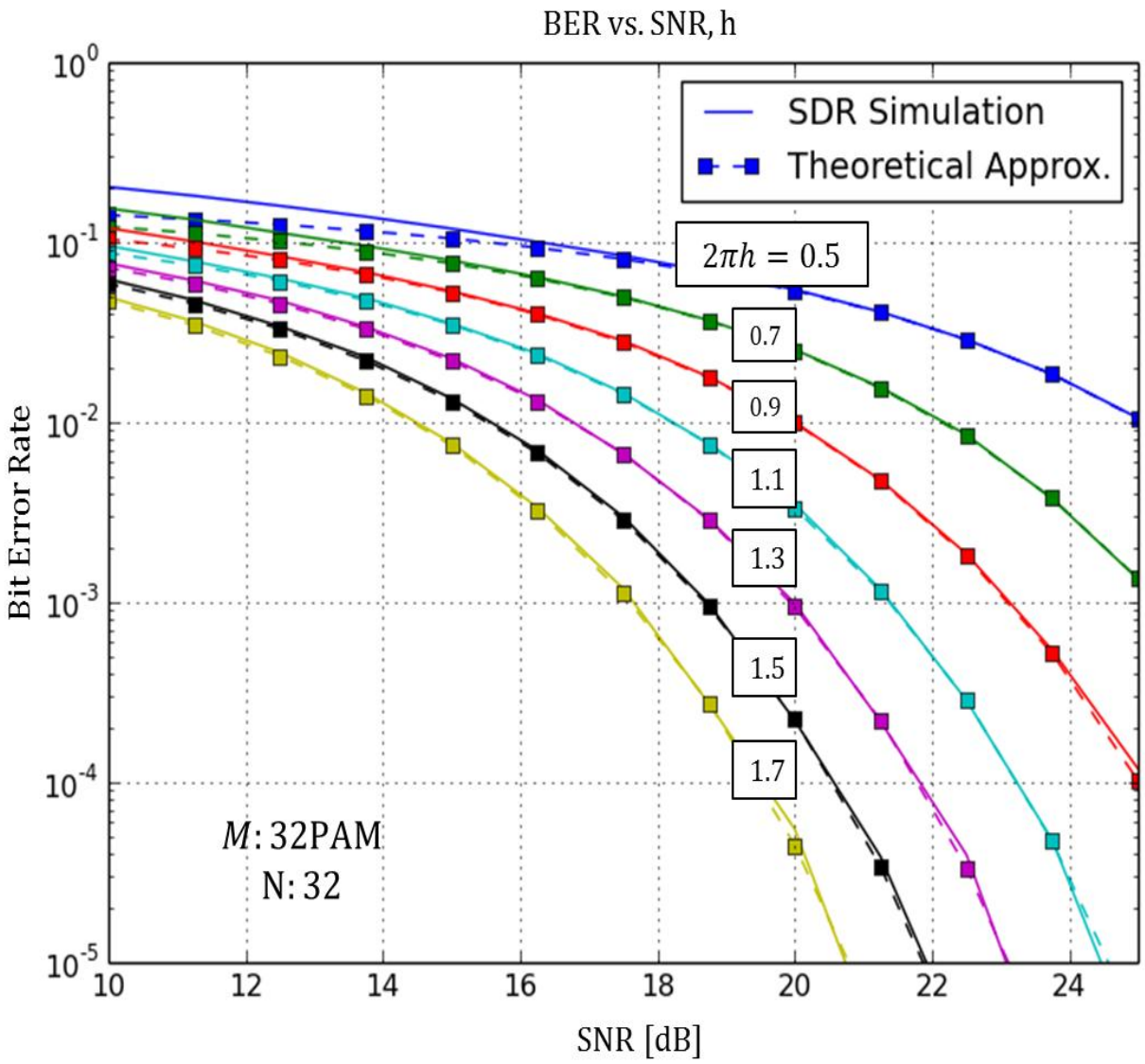

Figure 7.5: 32-PAM, N=32, os factor=8

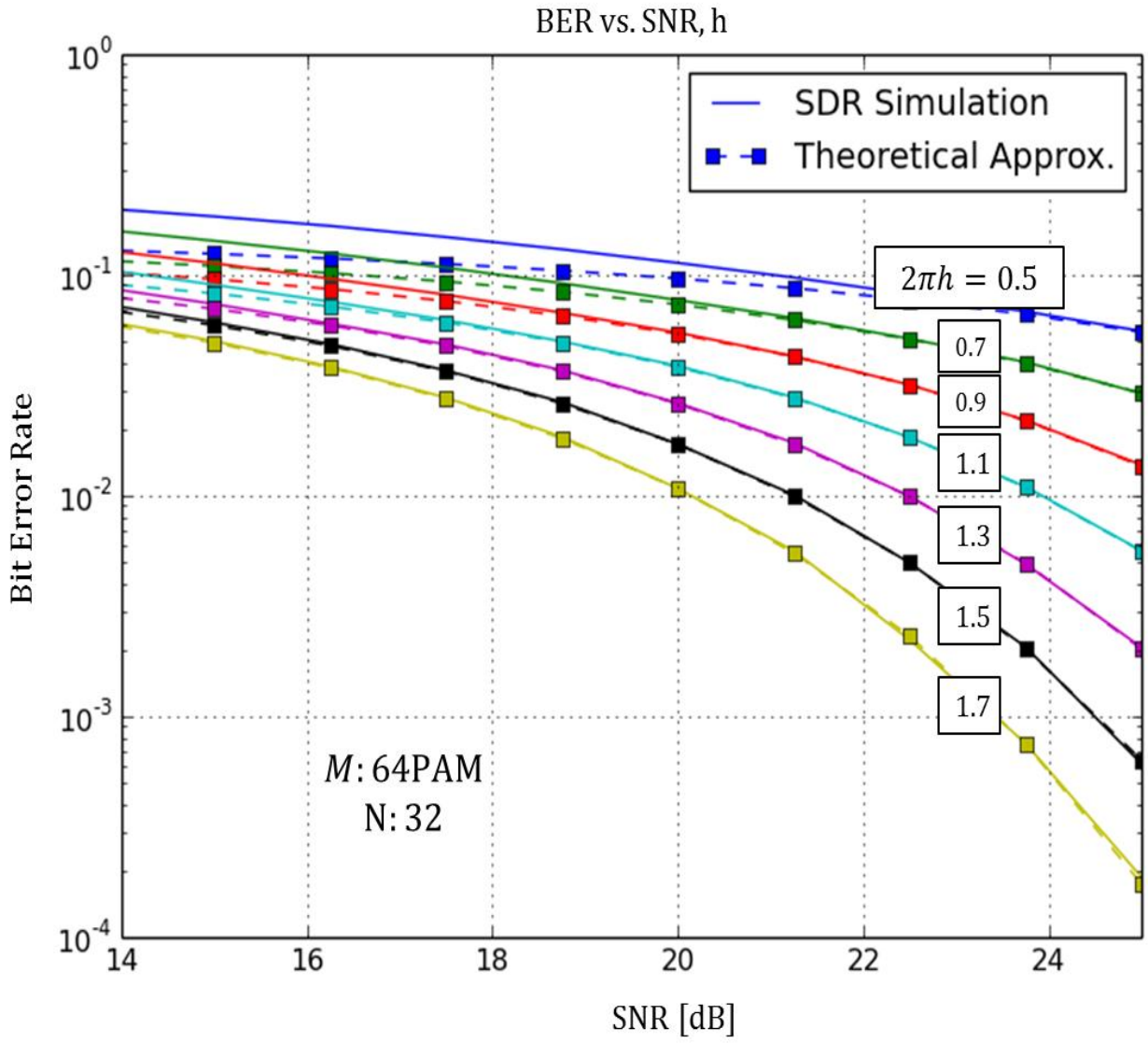

Figure 7.6: 64-PAM, N=32, os factor=8

The Figures 7.3 through 7.6 show that the GNU Radio CE-OFDM implementation performs very close to the theoretical approximation, for SNR levels above the FM threshold (> 10 dB). The FM threshold effect can be observed more prominently in the lower modulation indices of the 32 and 64-PAM simulations, as the curves of the simulated data begin to deviate from the theoretical approximation before the 10 dB threshold.

8 CONCLUSIONS

In this thesis, the CE-OFDM waveform was examined as a solution to the high peak-to-average-power ratio (PAPR) problem of OFDM. CE-OFDM averts the necessity for highly linear, power-inefficient amplification of OFDM by employing phase modulation to transform the high-PAPR multicarrier signal into a constant envelope signal, like FSK or GMSK, which can be amplified with non-linear power amplifiers at near saturation levels of efficiency.

The primary contribution of this thesis was a highly tunable software-defined radio (SDR) implementation of the waveform which enables rapid-prototyping and testing of CE-OFDM systems. A software 'test bench' was created to enable rapid configuration and testing of the CE-OFDM waveform over all permutations of its parameters, over both simulated and physical RF channels, and the results of a baseband simulation of the CE-OFDM receiver in an AWGN channel validate the performance of the signal processing implementation. Thus, the SDR implementation of this thesis proves to be viable framework for prototyping and testing CE-OFDM systems.

8.1 Further Research

The following subsections include recommendations for extending and applying the SDR framework for further research.

8.1.1 Extending Waveform Implementation

Using the GNU Radio software framework a number of extensions can be readily added to the current waveform implementation. The waveform can be extended to include blocks for encoding/decoding, scrambling/de-scrambling, and equalization, to create a more sophisticated communications system.

8.1.2 Extending Simulation and Analysis

The waveform simulation testbench can be extended to test error rate performance and spectral efficiency of the waveform over a number of modulation parameters, coding rates and decoder algorithms, equalization techniques, and multipath channel models to perform in-depth and multivariate analysis of waveform performance.

8.1.3 RF Testing

The current CE-OFDM transmitter and receiver implementations can be extended to transmit and receive CE-OFDM signals over-the-air using USRP SDR front-ends. Figure 8.1 displays transmitter and receiver flowgraphs of a fully-functional radio system.

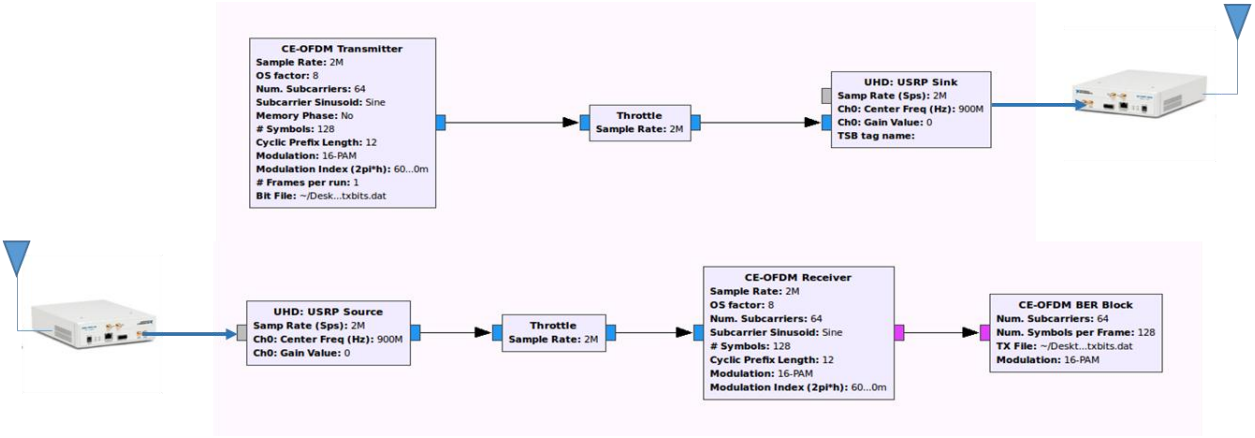

Figure 8.1: GNU Radio Flowgraphs of RF CE-OFDM System

8.1.4 Improving Computational Efficiency

Real-time transmission and reception of the waveform requires the modulation and demodulation of CE-OFDM frames to meet computation time requirements. The latter requires optimizing computational efficiency of the modulation and demodulation routines. The most time-intensive processes of the waveform are the subcarrier modulation and subcarrier correlation stages of the transmitter and receiver respectively. Using an Inverse and Forward Discrete Sine Transform, the respective computations of subcarrier modulation and correlation can be performed in FPGA hardware for significantly improved computational efficiency. Benchmarks of waveform computation time must be studied for a number of sample rates.

8.1.5 Cognitive Radio Integration

The various performance tuning parameters of CE-OFDM waveform make it an attractive platform for cognitive radio research.

9 REFERENCES

[1] Ahmed, Ahsen, Steve Thompson, and James Zeidler. "Constant Envelope OFDM with Channel Coding." *Milcom 2006* (2006)

[2] Ahmed, Ahsen U., Steve C. Thompson, David W. Chi, and James R. Zeidler. "Subcarrier Based Threshold Performance Enhancement in Constant Envelope OFDM." *MILCOM 2012 - 2012 IEEE Military Communications Conference* (2012).

[3] Bogucka, Hanna, and Andrea Conti. "Degrees of Freedom for Energy Savings in Practical Adaptive Wireless Systems." *IEEE Commun. Mag. IEEE Communications Magazine* 49.6 (2011): 38-45.

[4] Carroll, Aaron, and Gernot Heiser. "An Analysis of Power Consumption in a Smartphone." (n.d.).

[5] "Daughterboard Properties." *USRP Hardware Driver and USRP Manual: Daughterboards*. N.p., n.d. Web. <http://files.ettus.com/manual/page_dboards.html>.

[6] Joung, Jingon, Chin Keong Ho, and Sumei Sun. "Spectral Efficiency and Energy Efficiency of OFDM Systems: Impact of Power Amplifiers and Countermeasures." *IEEE J. Select. Areas Commun. IEEE Journal on Selected Areas in Communications* 32.2 (2014): 208-20.

[7] Mestdagh, Dennis J. G, PhD. "Reduction Peak-to-Average-Power-Ratio of OFDM Systems: A Tutorial Overview." *Academia*. N.p., Oct. 2014.

[8] Reed, Jeffrey Hugh. "Characteristics and Benefits of a Software Radio." *Software Radio: A Modern Approach to Radio Engineering*. Upper Saddle River, NJ: Prentice Hall, 2002. 4.

[9] *SBX-40 400 MHz*. Ettus Research, n.d. Web. <https://www.ettus.com/product/details/SBX>.

[10] Talbot, David. "Efficiency Breakthrough Promises Smartphones That Use Half the Power." *MIT Technology Review*. N.p., 31 Oct. 2012.

[11] Thompson, S.c., A.u. Ahmedt, J.g. Proakis, and J.r. Zeidler. "Constant Envelope OFDM Phase Modulation: Spectral Containment, Signal Space Properties and Performance." *IEEE MILCOM 2004. Military Communications Conference, 2004.* (n.d.): n. pag. Web.

[12] Thompson, Steve, Ahsen Ahmed, John Proakis, James Zeidler, and Michael Geile. "Constant Envelope OFDM." *IEEE Transactions on Communications IEEE Trans. Commun.* 56.8 (2008): 1300-312.

[13] Thompson, Steve C. *Constant Envelope OFDM Phase Modulation*. Diss. U of California, San Diego, 2005.

[14] "USRP2 and N2x0 Series Features List." *USRP Hardware Driver and USRP Manual: USRP2 and N2x0 Series*. Ettus Research, n.d. Web. <http://files.ettus.com/manual/page_usrp2.html>.

[15] Varahram, Pooria, Borhanuddin Mohd. Ali, and Somayeh Mohammady. "Power Amplifiers in Wireless Communications." *Power Efficiency in Broadband Wireless Communications*. N.p.: CRC, 2014. 23-59. Print.

[16] "What Is GNU Radio and Why Do I Want It?" *WhatIsGR*. N.p., n.d. Web. <https://gnuradio.org/redmine/projects/gnuradio/wiki/WhatIsGR>.

[17] Yang, Samuel C. "Time Dimension: Multipath Delay Spread." *OFDMA System Analysis and Design*. Boston: Artech House, 2010. 30.

[18] Robertson, Andrew, et al. *A Constant Envelope OFDM Implementation on GNU Radio*. No. NRL/MR/5524--15-9575. Naval Research Lab Washington DC Networks and Communication Systems Branch, 2015.

[19] "NI USRP-2920 Block Diagram." *National Instruments*. N.p., n.d. Web. <http://zone.ni.com/reference/en-XX/help/373380B-01/usrphelp/2920_block_diagram/>.

[20] Rosu, Iulian. "RF Power Amplifiers." *RF Technical Articles*. YO3DAC - VA3IUL, n.d. Web. <http://www.qsl.net/va3iul/>.

[21] Thompson, Steve, John Proakis, James Zeidler, and Michael Geile. "Constant Envelope OFDM in Multipath Rayleigh Fading Channels."*Milcom 2006* (2006): n. pag. Web.

[22] Ahmed, Ahsen U., Steve C. Thompson, and James R. Zeidler. "Threshold Extending Receiver Structures for CE-OFDM." *MILCOM 2007 - IEEE Military Communications Conference* (2007)